Available online www.unicrossjournals.com

UNICROSS JOURNAL OF SCIENCE AND TECHNOLOGY, UJOST

RESEARCH ARTICLE VOL. 5(1) MARCH , 2026 ISSN:2814-2233

Date Approved March 31, 2026 Pages 1 – 42

HARNESSING THE THERMOGENIC POTENTIAL OF THE LITHOLOGICAL BOWELS OF OGUN STATE, SOUTH-WESTERN, NIGERIA

Ogunsanwo F.O.[1*], Adelaja A.D.[1], Osinubi A.D.[2] and Adepitan J.O.[1]

[1.] Physics Department, Tai Solarin Federal University of Education, Ijagun, Ogun State Nigeria

[2.] Chemical Sciences Department, Tai Solarin Federal University of Education, Ijagun, Ogun State Nigeria

Email: ogunsanwofo@tasued.edu.ng *

Abstract

This study assesses subsurface heat generation using airborne gamma-ray radiometric data across Ogun State, Nigeria, covering the three major lithological units: basement, weathered basement, and sedimentary terrains. Ten airborne radiometric datasets obtained from the Nigerian Geological Survey Agency were analyzed to evaluate radiogenic heat production (HP) across these lithologies using the Rybach model. Spatial distribution of HP was visualized through 2D and 3D surface maps generated in MATLAB, while anomalies were identified using box-and-whisker plots and histograms. Proximal heat sources were further examined using inferential and multivariate statistical analyses, and the influence of climatic parameters; temperature (T) and relative humidity (RH) on HP was investigated. The results indicate that mean HP values for basement units range from 5.20 to 12.53 $\mu W\, m^{-3}$ (A1–A4), while weathered basement units range from 3.18 to 6.69 $\mu W\, m^{-3}$ (W1–W3), and sedimentary units range from 3.63 to 8.89 $\mu W\, m^{-3}$ (R1–R3). All lithologies exhibit heat production above the International Atomic Energy Agency (IAEA) recommended limit of 4.0 $\mu W\, m^{-3}$, except for two units (W2 and R1). Linear regression analysis shows that neither temperature nor relative humidity significantly influence HP. The spatial distribution of anomalous HP closely correlates with lithology and mineralogical composition: granitic and migmatitic basement rocks serve as primary heat sources, weathered basement rocks act as secondary concentrators, and sedimentary units reflect varying degrees of dilution or basement inheritance. Hence, the results demonstrate that lithology and mineralogy are the dominant controls on radiogenic heat production, and the study area exhibits significant geothermal potential suitable for exploration.

Keywords: Lithological; Rybach model; Radiometric; Climatic parameters; Airborne Survey

1.0 Introduction

The growing global demand for sustainable and low-carbon energy sources has intensified interest in geothermal energy as a reliable alternative to fossil fuels. Unlike solar and

wind energy, geothermal energy provides a stable and continuous power supply that is largely independent of climatic variability (Haeger *et al.,* 2022; Bezuidenhout, 2023; Jabbarova *et al.,* 2024). Radiogenic heat production within the Earth's crust, generated primarily by the decay of naturally occurring radioactive elements such as uranium (U), thorium (Th), and potassium (K), constitutes a fundamental component of geothermal resources (Artemieva *et al.,* 2017; Ogunsanwo *et al.,* 2023). Understanding the spatial distribution and lithological controls of this heat is therefore critical for assessing geothermal potential, particularly in regions with limited subsurface temperature measurements.

Nigeria, despite its increasing energy demand and recurrent power deficits, remains largely unexplored in terms of geothermal energy development. Energy supply in the country is dominated by fossil fuels, exposing the economy to environmental degradation, price volatility, and supply insecurity (Goodge, 2018, Burton-Johnson *et al.,* 2020; Yusuf *et al.,* 2023). Southwestern Nigeria, including Ogun State, is underlain by a complex assemblage of Precambrian basement rocks, weathered basement units, and sedimentary sequences (Rahaman, 1976; Elueze, 1981; Ogunsanwo *et al.,* 2019; Olowofela *et al.,* 2019), all of which possess varying capacities for radiogenic heat generation. However, the thermogenic potential of these lithological units remains poorly quantified, resulting in a critical knowledge gap that hampers informed geothermal exploration and energy planning.

Previous geothermal investigations in Nigeria have focused largely on surface manifestations such as warm springs and regional heat-flow estimations (Hasterok *et al.,* 2018; Hazzard *et al.,* 2023; Ogunsanwo *et al.,* 2021; Ogunsanwo *et al.,* 2025), with limited integration of radiometric data for quantitative heat-production assessment. Airborne gamma-ray radiometry offers a robust and cost-effective means of estimating radiogenic heat production over large areas by mapping the spatial distribution of U, Th, and K within surface and near-surface rocks (Ashwal *et al.,* 1987; Telford *et al.,* 1990; Minty, 1997). When integrated with lithological mapping and statistical analysis, radiometric methods provide valuable insights into the geological controls on subsurface heat generation, especially in regions lacking deep borehole data.

Ogun State represents a strategic geological setting for geothermal assessment due to its juxtaposition of crystalline basement, weathered basement, and sedimentary terrains. These lithological "bowels" exhibit contrasting mineralogical compositions and structural frameworks that influence heat production, retention, and redistribution. Granitic and migmatitic basement rocks are typically enriched in heat-producing elements, while weathered equivalents may act as secondary concentrators. Sedimentary units, on the other hand, may exhibit diluted heat signatures or reflect inherited thermal characteristics from the underlying basement (Jaupart *et al.,* 2016; Hu *et al.,* 2019). Despite this geological diversity, no comprehensive, lithology-based evaluation of radiogenic heat production has been conducted for the state.

This study is therefore justified by the need to (i) quantitatively evaluate radiogenic heat production across the major lithological units of Ogun State, (ii) establish the spatial relationship between heat anomalies and mapped lithologies, and (iii) assess the relative influence of geological and climatic factors on subsurface heat generation. By employing airborne gamma-ray radiometric data, the Rybach heat-production model, spatial visualization techniques, and multivariate statistical analysis, the study provides a systematic framework for identifying geothermal-favorable zones in a data-limited environment.

From an economic and developmental perspective, harnessing geothermal energy in Ogun State could contribute significantly to Nigeria's energy diversification strategy. Localized geothermal resources may support decentralized power generation, industrial heat supply, and rural electrification, thereby reducing reliance on fossil fuels and enhancing energy security. Furthermore, identifying high heat-production zones has implications beyond energy generation, including mineral exploration, crustal thermal modeling, and sustainable land-use planning. By characterizing the thermogenic potential of the lithological units in Ogun State, this study offers a scientific basis for geothermal prospecting and provides a template for similar assessments across other parts of the Nigerian Basement Complex.

1.1 Geological setting of the lithological bowels

Ogun State lies between latitudes 6°30′N and 7°50′N and longitudes 3°00′E and 4°30′E, covering an area of about 16,400 km². The region experiences a tropical climate with alternating wet and dry seasons, which affects the accessibility of some outcrops during field operations. Structurally, the area is characterized by gentle folding and faulting associated with the rifting that formed the Dahomey Basin (Olatinsu *et al*., 2022)

Table 1 presents the airborne geological classification and summarizes the ten lithological units in Ogun State assessed for radiogenic geothermal potential, grouped into basement, weathered basement, and sedimentary terrains after Rahaman (1989), Cooray, (1972), Rahaman, (1976); Elueze, (1981) and Dada *et al.* (1989). The classification reflects both the compositional diversity and spatial extent of the lithological units, as indicated by the large number of airborne samples (303,101), which enhances the statistical robustness of the geothermal assessment.

The basement terrain, represented by units A1–A4, is dominated by Precambrian crystalline rocks, including migmatites, amphibolite schists, quartzite schists, biotite–garnet schists, granodiorites, and porphyritic granites. These lithologies are typically enriched in radiogenic elements such as uranium (U), thorium (Th), and potassium (K), particularly within felsic components like migmatites and granites. Unit A4 (Olodo), composed almost entirely of migmatite, is of particular geothermal interest due to the known association between migmatitic rocks and elevated radiogenic heat production. Similarly, the compositional complexity of A1–A3 suggests heterogeneous heat production patterns controlled by mineralogical variations and tectono-metamorphic history. The relatively large sample counts within these

units further support detailed spatial analysis of radiogenic heat variability within the basement domain.

The weathered basement units (W1–W3) represent transitional zones where crystalline basement rocks are overlain or altered by sedimentary materials and intense tropical weathering. These units comprise mixed lithologies, including sandstone–limestone associations, shale, recent alluvium, coastal plain sands, and residual basement rocks. The compositional heterogeneity of the weathered basement introduces significant variability in radiogenic heat estimates, as weathering processes can redistribute or attenuate radioactive element concentrations. Units W1 and W2, with the highest sample densities, provide valuable insight into how surface processes and sediment cover influence gamma-ray responses and heat production estimates, making them critical for evaluating the performance differences between field-based and airborne surveys.

The sedimentary terrain (R1–R3) is dominated by shale–limestone sequences, sand–clay–shale assemblages, coastal plain sands, and recent alluvial deposits. These lithologies generally exhibit lower radiogenic heat production compared to basement rocks due to reduced concentrations of U, Th, and K, particularly in quartz-rich sands and unconsolidated sediments. However, shale- and limestone-rich units such as R1 (Ewekoro) and R3 (Oja–Odan) may locally enhance radiogenic heat signatures due to clay mineral content and diagenetic enrichment. The sedimentary units therefore provide an important contrast to the basement and weathered basement terrains, allowing assessment of lithology-controlled heat production and survey sensitivity across different geological settings.

Generally, the lithological underlying rocks were characterized (Table 1), which thereby highlights the geological complexity of Ogun State and establishes a strong framework for interpreting spatial variations in radiogenic heat production. The diversity of lithological compositions, coupled with extensive airborne sampling, enables a robust comparison of field-based and airborne heat estimates across contrasting geological environments. This classification underpins subsequent analyses by linking radiogenic heat behavior to lithology, weathering intensity, and sedimentary processes, which are critical factors in geothermal assessment and crustal heat-flow studies.

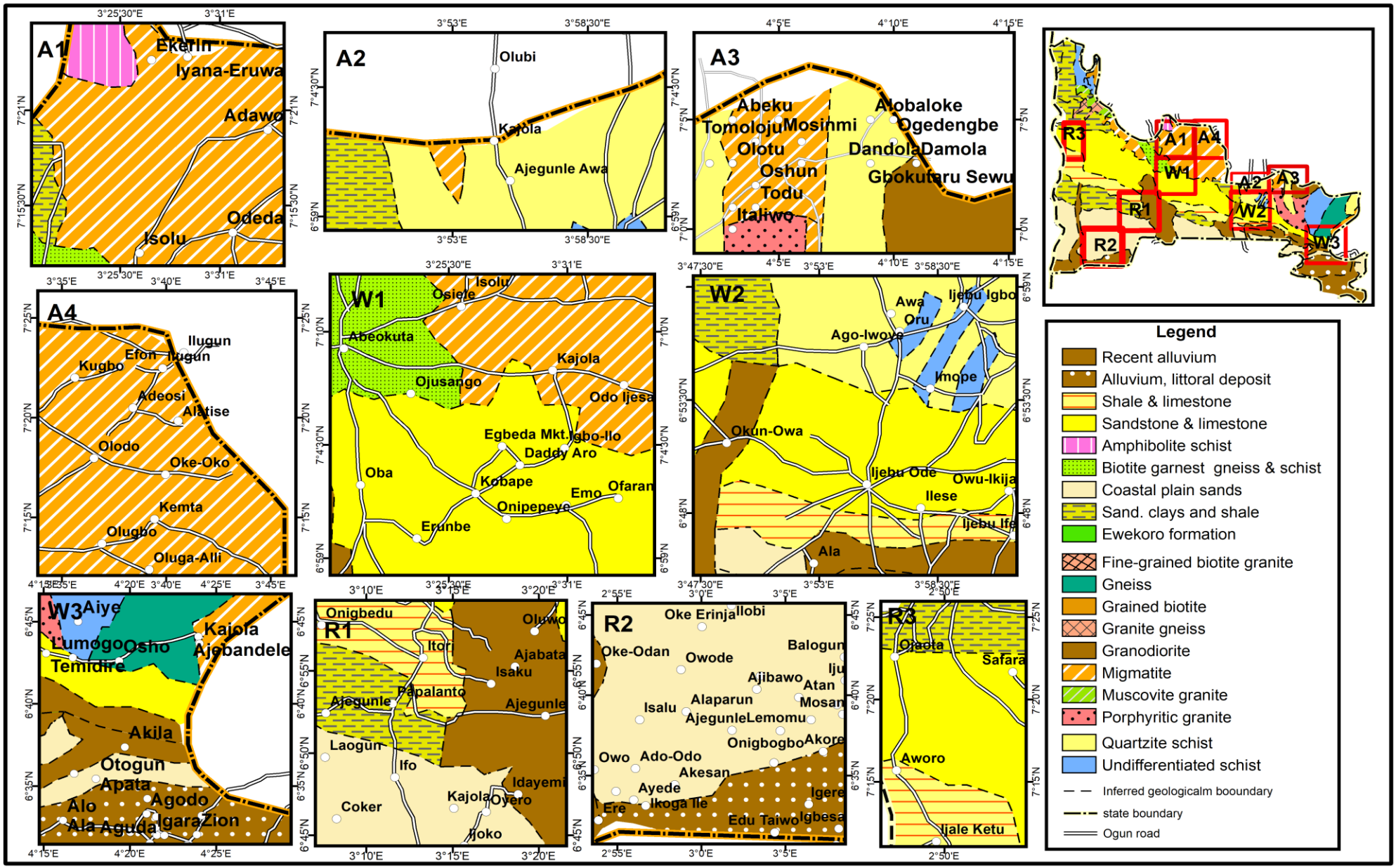

Fig. 1 Lithological classification of underlying stratified bedrock composition for thermal prospect

Table 1: The Airborne geological classification and the ten lithological units assessed for geothermal potential

Lithological Formations	Zone	Units Code	Bedrock Composition	N Samples
Basement	Odeda	A1	Migmatite, Amphibiote schist, Biotite garnet schist	38, 672
	Kajola	A2	Migmatite, Quazite schist, Undifferenciated schist	16, 228
	Ijebu - Igbo	A3	Migmatite, Porphyritic granite, Quazite schist, granodiorite	20, 929
	Olodo	A4	Migmatite	25, 103
Weathered Basement	Abeokuta	W1	Sandstone + Limestone, migmatite, Biotite garnet gneiss schist, granodiorite	40, 000
	Ijebu - Ode	W2	Sandstone +Limestone, Undifferenciated schist, Recent Alluvium, Shale+Limestone,	40, 007
	Ogbere	W3	Porphyritic granite, Undifferenciated schist, Migmatite, Sandstone + Limestone, Coastal plain sand, recent alluvium, Alluvium littoral deposit	26, 475
Sedimentary	Ewekoro	R1	Shale + limestone, , Coastal plain sand, recent alluvium, Sand+Clay +Shale	39, 784
	Atan - Ota	R2	Coastal plain sand, recent alluvium	40, 000
	Oja - Odan	R3	Sand + Clay +Shale, Sandstone +Limestone, Shale + limestone	15, 903
				303,101

2.0 Materials and methods

The research involves airborne radiometric surveys conducted using portable gamma-ray spectrometers calibrated for the detection of uranium (U), thorium (Th), and potassium (K) concentrations, which are key contributors to natural crustal heat generation. Data obtained from these measurements were used to compute radiogenic heat production and total heat generation, which were subsequently analyzed to produce spatial maps of geothermal anomalies across the study area.

2.1 Airborne –based data

The airborne radiometric data used was collected from the archive of Nigeria Geological Survey Agencies, Abuja, Nigeria. Airborne radiometric surveying involves systematic measurement of natural gamma radiation emitted from rocks and soils at or near the Earth's surface. The survey was carried out using fixed-wing aircraft equipped with high-sensitivity NaI (sodium iodide) crystal detectors, a data acquisition system, and appropriate navigation instrumentation. The detectors were calibrated to record gamma-ray counts corresponding to the three principal radiometric channels; potassium (K), uranium (U), and thorium (Th) measurements. To ensure precision, the aircraft was flown at a nominal terrain clearance of 80–120 m, with a flight line spacing of approximately 500 m and tie lines typically spaced at 2,000 m. The acquired radiometric data were subsequently gridded, processed and computed for heat production across each lithological unit.

2.2 Meteorological data

The climatic parameters such as temperature and humidity were obtained for the available stations in Ogun state for the year 2024 from the Nigerian Meteorological station (NIMET), Bill Clinton Drive, Nnamdi Azikiwe International Airport, Abuja, Nigeria. These datasets were chosen due to their reliability and suitability for climatological and energy assessments.

2.3 Analysis of data

Heat production

In this study, the model for calculating radiometric heat content from the earth crust using HPEs was used as given by Rybach (1988); IAEA, (2003); Ogunsanwo *et al* (2021); Hazzard and Richards (2024) in equation (1)

$$HP(\mu W m^{-3}) = \rho\,(9.52C_U + 2.56C_{Th} + 3.48C_K) \times 10^{-5} \quad (1)$$

where ρ is the bulk density of rock in kg m^{-3}; C_U and C_{Th} represent the uranium and thorium concentrations present in the rocks in ppm; and C_K represents potassium concentration in % . The density of the individual lithological units was used following the work of Telford *et al.* (1990).

2.4 Linear regression model Estimation

Linear regression model was developed between heat generated and the climatic factors such as surface temperature and relative humidity in the form presented in Equation 2.

$$HP = aT + bRH + c \quad (2)$$

HP is the heat produced, T is the temperature, and RH is the relative humidity

2.5 Descriptive Statistical Analysis and Box Plot Trends

In order to describe the behaviour of heat produced and heat generated by aeroradiospectrometric approach, this study employ the use of box and whisker plot alongside the descriptive statistical parameters such as minimum, maximum, mean, standard deviation, kurtosis and skewness. Box plot gives a concise visual representation of data distribution.

2.6 Geothermal heat sources proximal Analysis

In order to examined the proximal sources analysis across the ten lithological units, inferential and multivariate statistical analysis were adopted. Two inferential statistical tools namely; T-test and F-test

were employed while principal component analysis (PCA) and cluster analysis were carried out for multivariate analysis. These analyses were performed with the aid of SPSS 20 software.

3.0 Results and Discussions

The geothermal results across the lithological units are presented in Figs. 2–11 using a combination of 2D contour maps and 3D surface plots to provide a comprehensive visualization of radiogenic heat distribution. The 2D contour maps effectively illustrate the lateral continuity, spatial gradients, and areal extent of heat production anomalies within each lithological unit, allowing direct comparison of heat intensity patterns across basement, weathered basement, and sedimentary terrains. This representation is particularly useful for identifying localized hotspots, boundary-controlled variations, and regional trends associated with lithological and structural controls. The complementary 3D surface plots translate the same datasets into vertical relief, enhancing the interpretation of anomaly magnitude, intensity contrast, and spatial heterogeneity that may not be readily apparent in plan-view maps alone. By visualizing heat production as topographic elevation, the 3D surfaces emphasize relative anomaly strength, isolate dominant heat-producing zones, and clarify transitions between background and anomalous regions. Together, the dual visualization approach improves interpretability, supports cross-validation of spatial patterns, and provides a robust framework for comparing geothermal characteristics across diverse lithological units.

3.1 Spatial distribution of radiogenic heat in basement unit (A1 – A4)

The 2D contour map (Fig. 2a) reveals a dominantly high heat production regime across much of the A1 unit, as indicated by extensive red to orange color zones corresponding to elevated heat values. These high-HP domains suggest significant enrichment of radiogenic elements (U, Th, and K), which is consistent with the felsic components of migmatites and biotite-rich schists present in the unit. Localized pockets of lower heat production, represented by green to blue contours, occur mainly along the southern and marginal portions of the map. These zones likely reflect lithological transitions, mafic intercalations, or zones of enhanced weathering and alteration that dilute radiogenic element concentrations. The contour patterns further indicate relatively smooth lateral gradients in some areas, punctuated by sharp transitions, implying heterogeneous mineralogical distribution and possible structural control such as shear zones or compositional banding within the basement complex.

The 3D surface plot (Fig. 2b) provides a more intuitive representation of the amplitude and geometry of heat production variations across the A1 unit. Prominent surface peaks correspond to the high-HP zones identified in the 2D map, highlighting discrete radiogenic “hotspots” that rise above the surrounding terrain. These peaks are interpreted as zones dominated by radiogenically enriched felsic lithologies or localized concentrations of potassium-bearing minerals. Conversely, the troughs and depressions in the surface plot coincide with areas of reduced heat production, reinforcing the interpretation of lithological heterogeneity and possible structural or weathering influences. The relatively uneven surface morphology confirms that radiogenic heat production within the A1 unit is not uniform but spatially controlled by compositional variability and geological architecture.

The spatial variation of radiogenic heat production within the A2 basement unit was presented in Figure 3 using (a) a 2D contour map and (b) a 3D surface plot. The 2D contour representation shows generally low to moderate

heat production across the unit, with isolated zones of elevated heat concentrated mainly toward the northern margin. These high-heat zones contrast with broad areas of comparatively lower heat intensity, indicating lateral heterogeneity within the A2 unit. The 3D surface plot further emphasizes this pattern by displaying a pronounced heat ridge along the northern sector, with heat values gradually decreasing southward. The surface is characterized by gentle undulations rather than sharp peaks, reflecting subdued heat variability relative to the A1 unit. Overall, the spatial patterns indicate that radiogenic heat production in the A2 unit is moderately distributed, with localized enhancements superimposed on a generally low-heat basement background.

The spatial distribution of radiogenic heat production within the A3 basement unit was constructed using (a) a 2D contour map and (b) a 3D surface plot (Fig. 4). The 2D contour map reveals predominantly moderate heat production across most of the unit, with a distinct high-heat zone concentrated toward the northeastern sector. This localized anomaly contrasts with the relatively uniform background heat levels elsewhere, indicating limited but significant spatial heterogeneity. The 3D surface representation further emphasizes this pattern by showing a pronounced, isolated heat peak rising above a generally subdued surface. Heat values decrease progressively away from this peak, forming a smooth gradient rather than abrupt fluctuations. The spatial patterns indicate that radiogenic heat production in the A3 unit is largely uniform but punctuated by localized zones of enhanced heat generation.

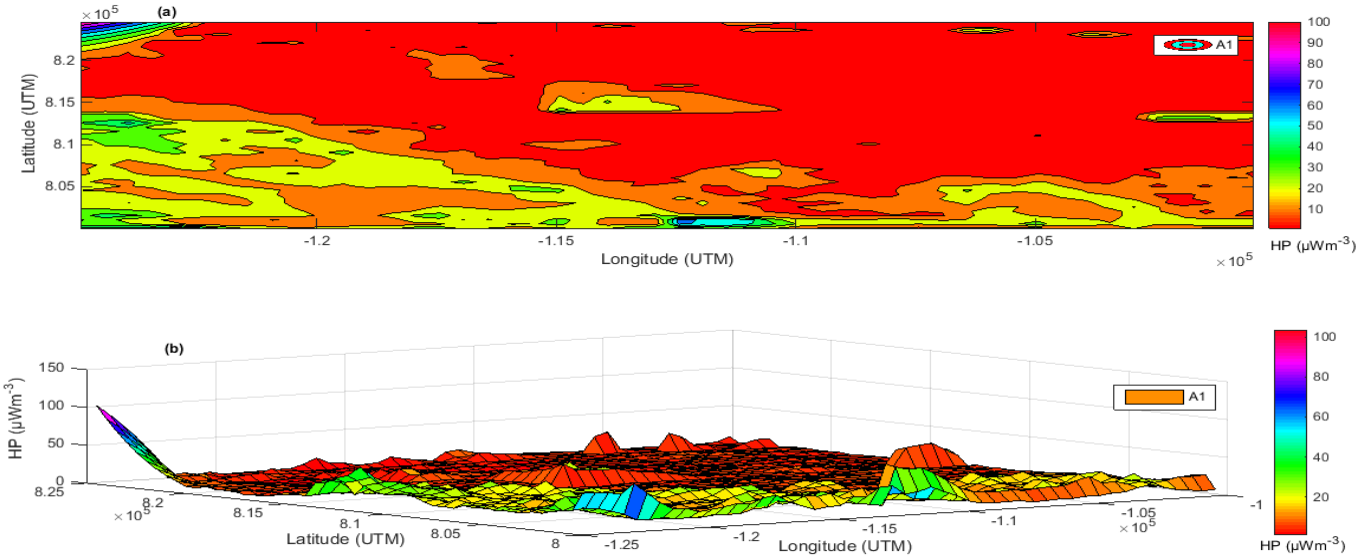

Fig. 2: Spatial representation of heat produced in (a) 2D contour (b) 3D Surface forms for A1 unit

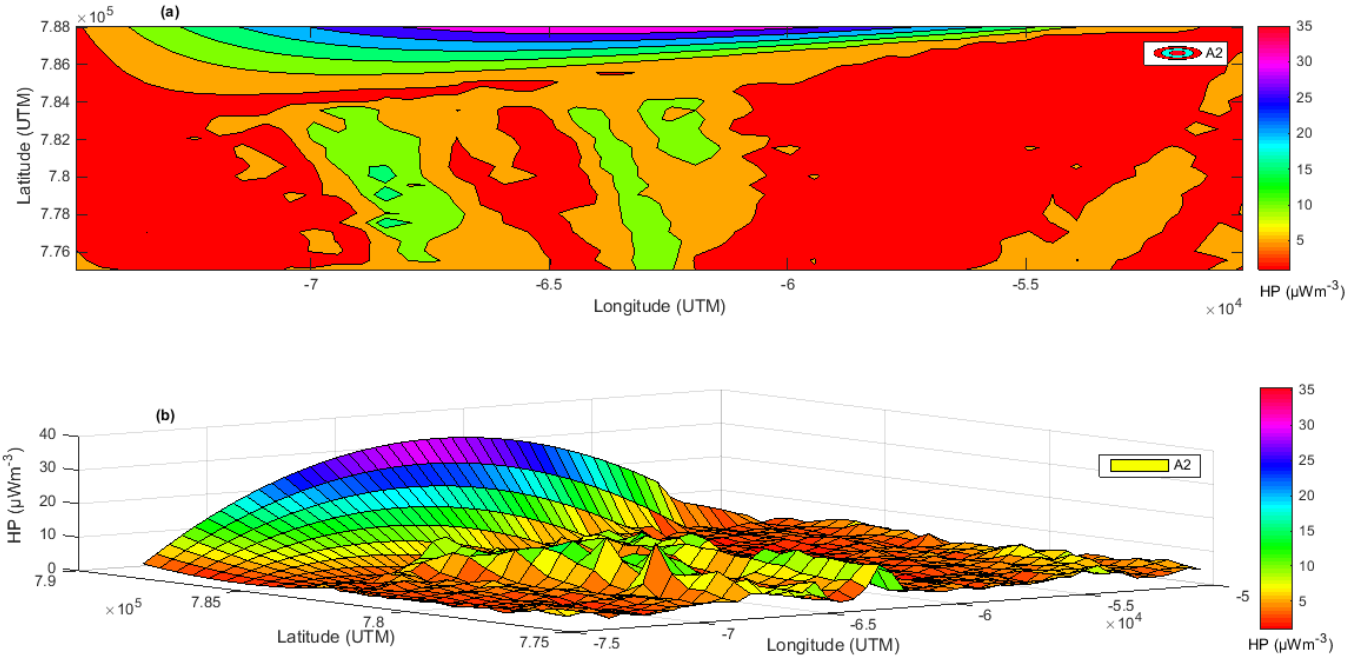

Fig. 3: Spatial representation of heat produced in (a) 2D contour (b) 3D Surface forms for A2 unit

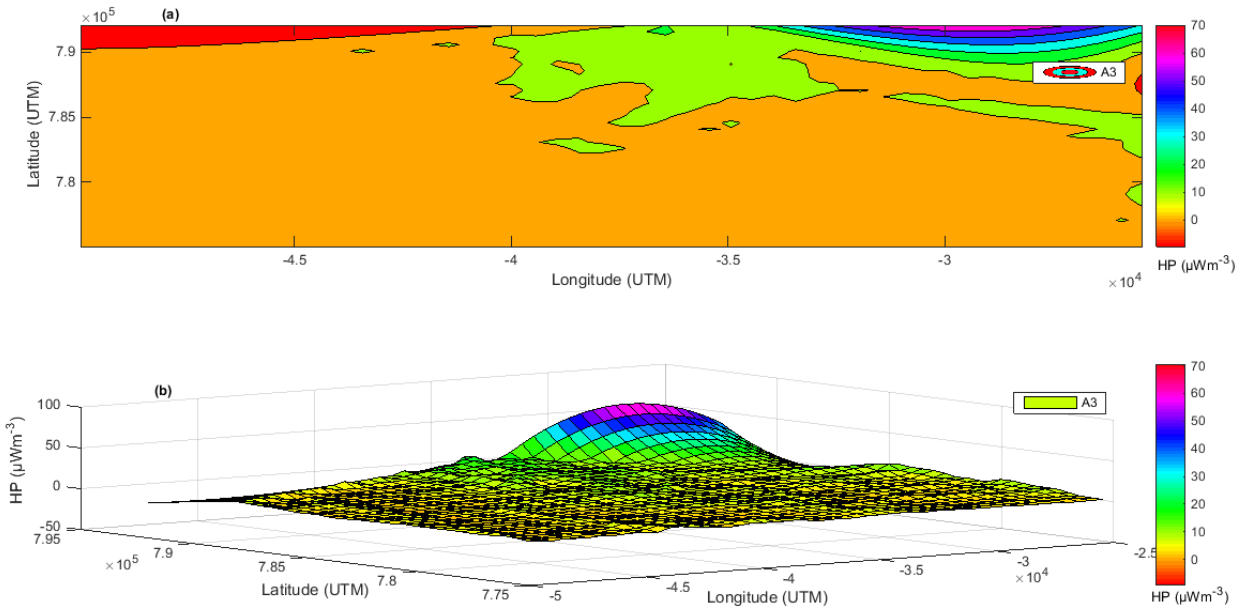

Fig. 4: Spatial representation of heat produced in (a) 2D contour (b) 3D Surface forms for A3 unit

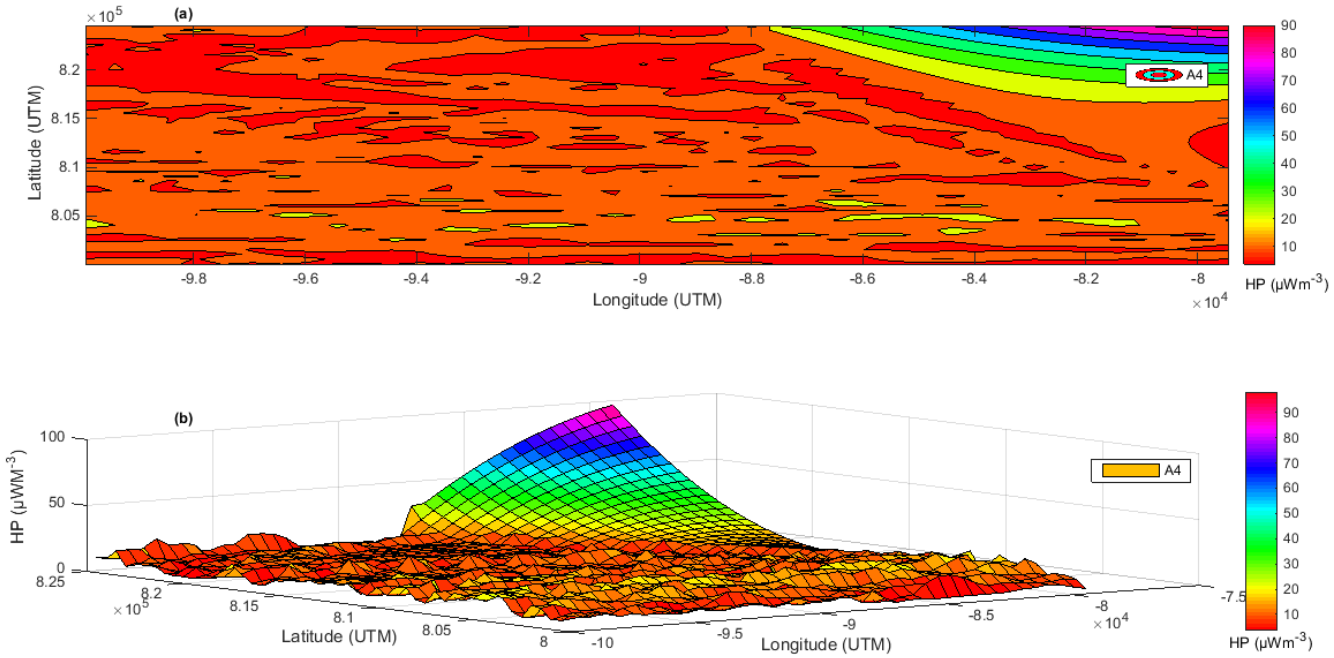

Fig. 5: Spatial representation of heat produced in (a) 2D contour (b) 3D Surface forms for A4 unit

Figure 5 shows the spatial distribution of radiogenic heat production (HP) in the A4 Basement unit using (a) a 2D contour map and (b) a 3D surface plot. Heat production is highly heterogeneous, with a pronounced high-intensity anomaly concentrated in the northeastern part of the area. HP values range from about 10 μW m^{-3} in background regions to nearly 90 μW m^{-3} within the localized hotspot, while most of the unit exhibits low to moderate heat production (10–30 μW m^{-3}). The 3D

surface plot highlights this anomaly as a steep, isolated peak rising above an otherwise flat radiometric basement, indicating strong local enrichment in radiogenic elements. Geologically, the localized high heat production likely reflects a radiogenic-rich granitic or pegmatitic intrusion, possibly controlled by basement structures or fracture zones that focused radiogenic mineralization.

3.2 Spatial distribution of radiogenic heat in weathered basement unit (W1 – W3)

The weathered basement units represent a transitional lithological layer between the fresh basement and the sedimentary cover, while they share similar statistical reliability, their spatial heat signatures (Figs. 6 – 8) show significant regional variation in both magnitude and location. The spatial distribution of radiogenic heat production (HP) in the W1 (Fig. 6) weathered basement unit was illustrated using (a) a 2D contour map and (b) a 3D surface representation. HP values range from approximately 5 μW m^{-3} to a maximum of about 35 μW m^{-3}. The 2D contour map shows a prominent high-heat anomaly in the north-central part of the area, with a general increase in heat production from the southern sector toward the north and minor localized highs along the eastern margin. The 3D surface plot highlights this anomaly as a pronounced ridge rising above a background heat level of roughly 10–15 μW m^{-3}. Unlike the sharp, isolated peak observed in the A4 basement unit, the W1 surface is more rugged, reflecting strong lateral variability in heat production. This heterogeneity is consistent with the complex nature of weathered basement terrains, where radiogenic elements are unevenly redistributed during chemical weathering processes. The reduced peak magnitude relative to the A4 basement suggests dispersion of heat-producing elements within the weathered profile.

Figure 7 illustrates the spatial distribution of radiogenic heat production (HP) within the W2 weathered basement unit using (a) a 2D contour map and (b) a 3D surface plot. Overall, heat production is markedly lower than in the A4 and W1 units, with peak values not exceeding ~10 μW m^{-3}. The 2D contour map shows a localized high-heat anomaly concentrated along the southern margin of the unit, while most of the area exhibits low and relatively uniform HP values of approximately 2–4 μW m^{-3}. The 3D surface representation emphasizes this pattern by depicting a subdued heat ridge along the southern edge, rising gently above an otherwise flat background. A sharp south-to-north gradient is evident, with heat values decreasing rapidly away from the anomaly and stabilizing across the central and northern sectors. Minor surface ruggedness reflects localized heterogeneity within the weathered profile, although overall heat amplitudes remain low. Geologically, the low maximum HP suggests depletion or redistribution of radiogenic elements during weathering, while the southern concentration of heat may reflect lithological contacts or structurally controlled zones that locally enhance radiogenic mineral accumulation.

Figure 8 shows the spatial distribution of radiogenic heat production (HP) in the W3 weathered basement unit using (a) a 2D contour map and (b) a 3D surface plot. Heat production values range from near 0 μW m^{-3} across most of the unit to a localized maximum of approximately 50 μW m^{-3}. The 2D contour map reveals a pronounced, isolated high-heat anomaly concentrated in the northeastern sector, while the remainder of the area exhibits uniformly low HP values, generally below 10 μW m^{-3}. The 3D surface representation highlights this anomaly as a sharp, steep peak rising from an otherwise flat radiometric background, emphasizing the highly localized nature of heat production in this unit. Compared to the rugged surfaces observed in W1 and W2, the W3 unit displays minimal lateral variability outside the main anomaly, indicating a relatively homogeneous

low-heat weathered cover. Geologically, the intense northeastern hotspot suggests the presence of an underlying high-heat-producing basement body, likely a granitic intrusion, whose radiogenic signature penetrates through the weathered layer with limited attenuation.

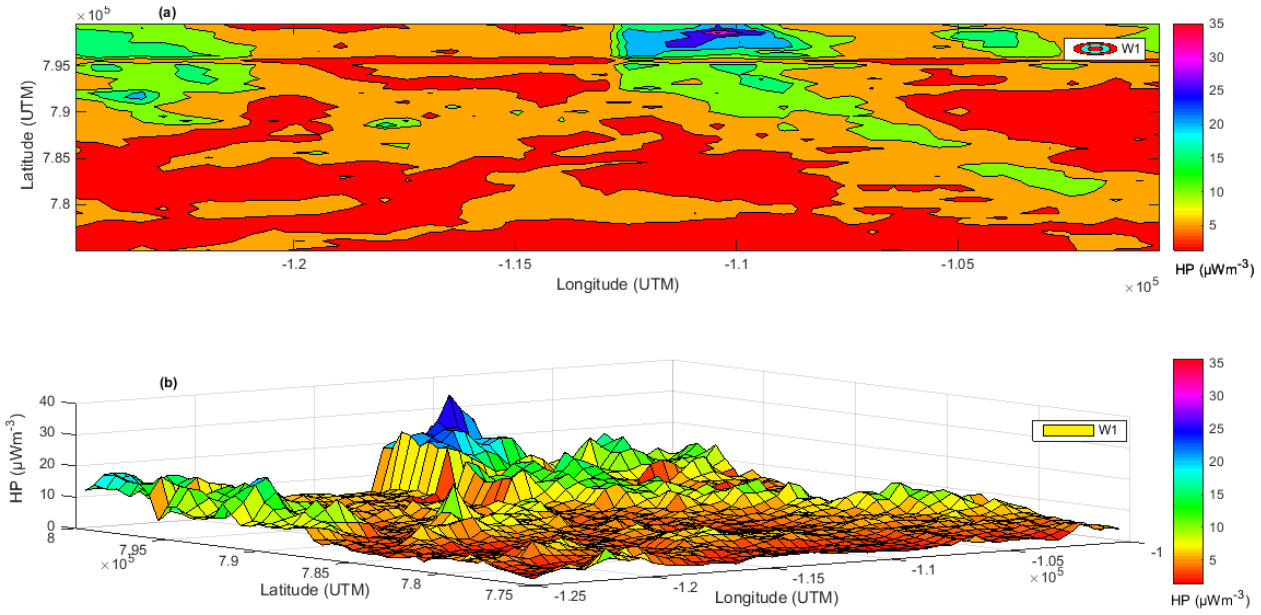

Fig. 6: Spatial representation of heat produced in (a) 2D contour (b) 3D Surface forms for W1 unit

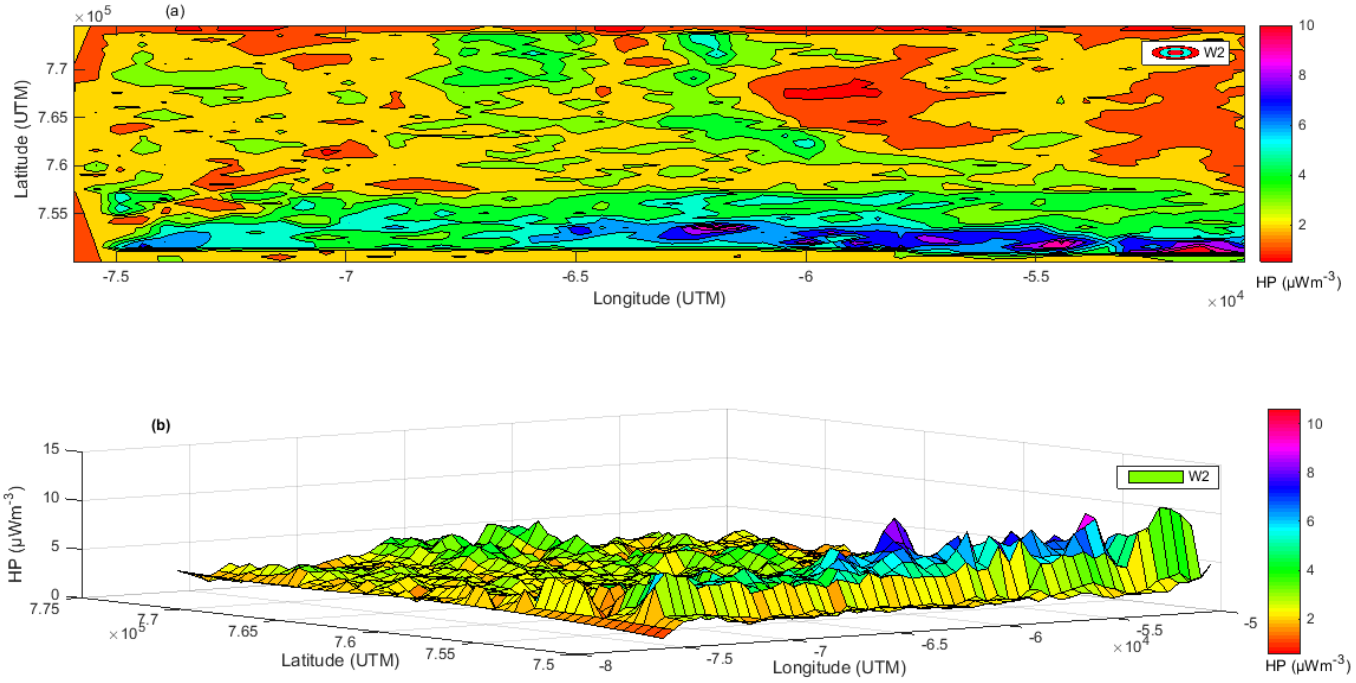

Fig. 7: Spatial representation of heat produced in (a) 2D contour (b) 3D Surface forms for W2 unit

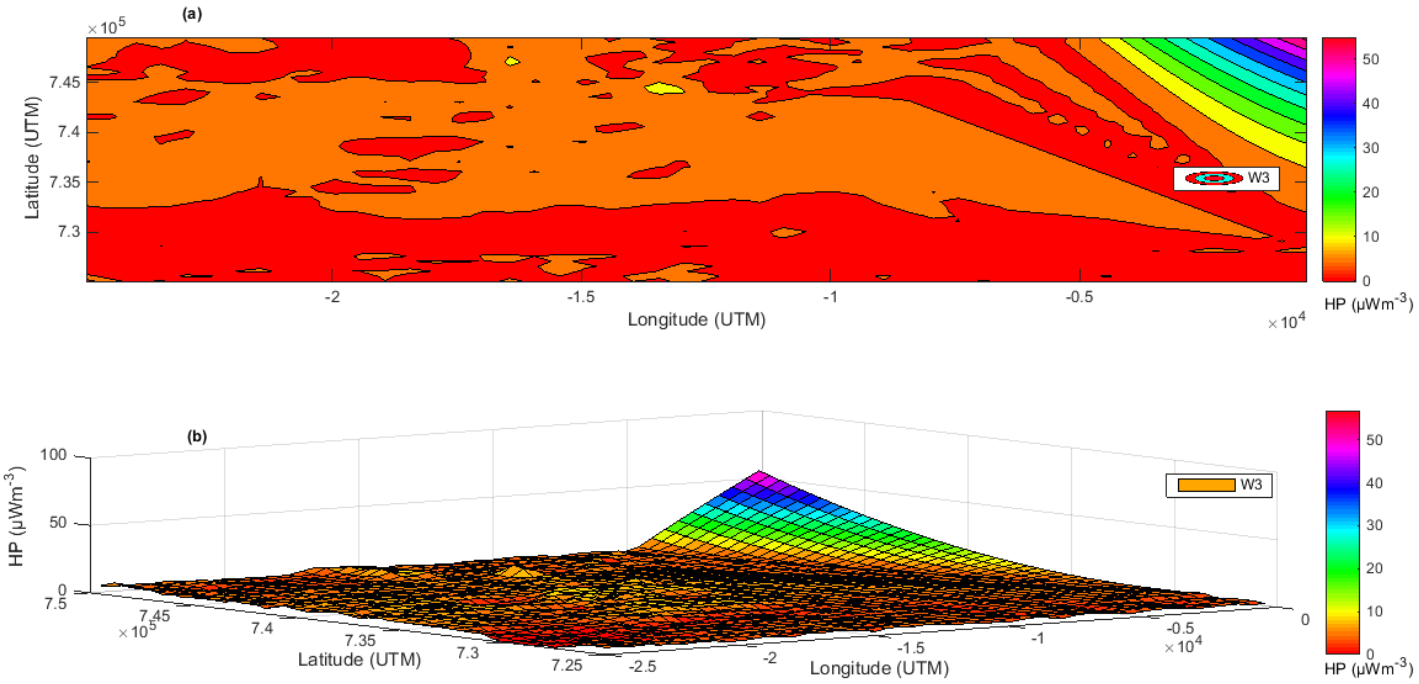

Fig. 8: **Spatial representation of heat produced in (a) 2D contour (b) 3D Surface forms for W3 unit**

3.3 Spatial Distribution of Radiogenic Heat in the Sedimentary Unit (R1- R3)

Figure 9 illustrates the spatial distribution of radiogenic heat production (HP) in the R1 sedimentary unit using (a) a 2D contour map and (b) a 3D surface plot. Heat production values are generally low, ranging from approximately 1 to 8 μW m^{-3}. The 2D contour map reveals a heterogeneous pattern, with relatively higher HP values (6–8 μW m^{-3}) concentrated along a central latitudinal band, while the northern and southern margins exhibit consistently lower heat levels of about 1–2 μW m^{-3}.The 3D surface representation emphasizes this variability through a rugged, low-relief surface characterized by numerous small peaks and troughs. The central high-heat band appears as an irregular, discontinuous ridge that rises only slightly above the surrounding sedimentary background. Compared to the basement and weathered basement units, the reduced amplitude and fragmented nature of the anomalies reflect the inherently low radiogenic potential of the sedimentary cover. The observed heat pockets are likely associated with localized clay-rich or heavy-mineral concentrations, while the overall low HP suggests that R1 primarily acts as a radiogenically inert layer, with minor contributions possibly influenced by underlying basement sources.

Figure 10 presents the spatial distribution of radiogenic heat production (HP) within the R2 sedimentary unit using (a) a 2D contour map and (b) a 3D surface representation. Heat production values are among the lowest observed in the study area, ranging from near 0 to approximately 9 μW m^{-3}. The 2D contour map reveals strong spatial heterogeneity, with a pronounced low-heat zone (0–2 μW m^{-3}) along the western margin and scattered moderate heat patches (6–8 μW m^{-3}) mainly in the north-central and eastern sectors. The 3D surface plot highlights this pattern as a highly rugged, low-relief

surface characterized by numerous small peaks and depressions. A distinct western trough is clearly defined, while the remainder of the unit displays subdued and discontinuous heat anomalies. The limited vertical relief confirms the absence of major radiogenic sources within the R2 sedimentary layer. The fragmented heat distribution reflects depositional heterogeneity, where variations in sediment composition and grain size control localized enrichment or depletion of radiogenic elements.

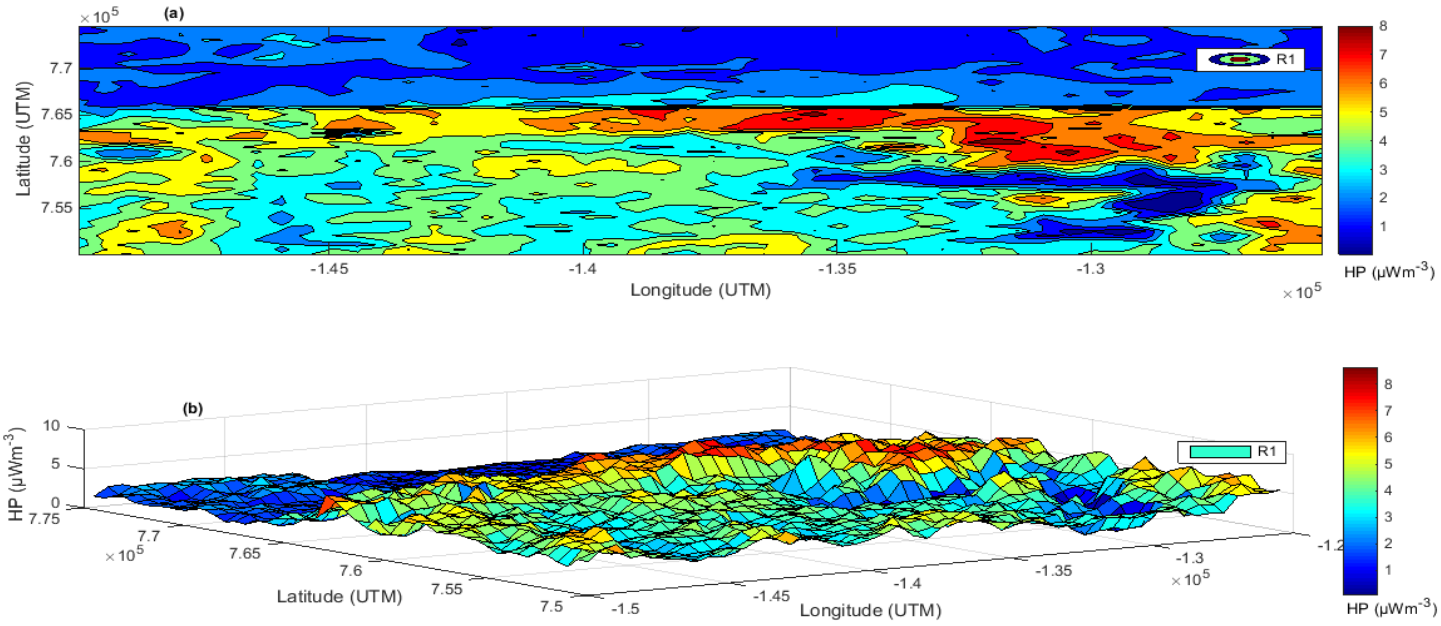

Fig. 9: Spatial representation of heat produced in (a) 2D contour (b) 3D Surface forms for R1 unit

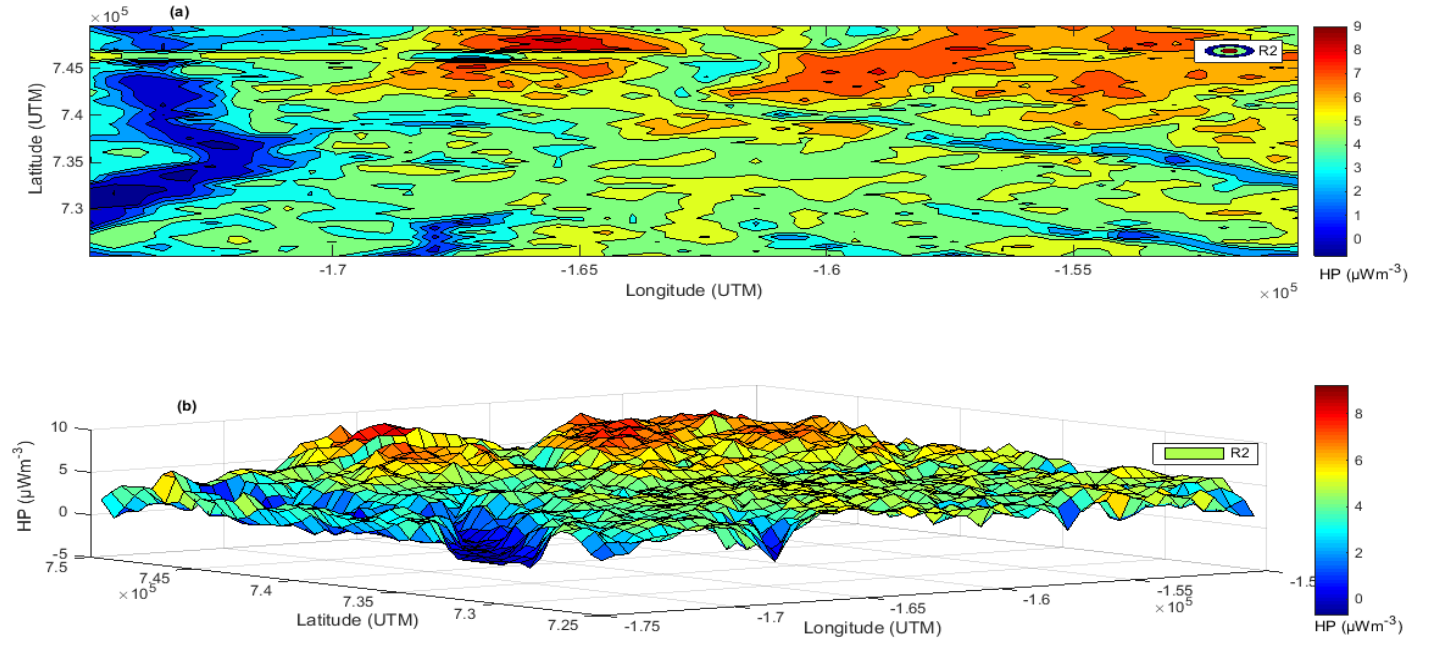

Fig. 10: Spatial representation of heat produced in (a) 2D contour (b) 3D Surface forms for R2 uni

The spatial distribution of Heat Production (HP) in the R3 sedimentary unit was constructed such that the 2D Contour Map (Fig. 11a) reveals a distinct latitudinal zonation, contrasting with the more chaotic HP patterns observed in R1 and R2. The northern section forms a "cold" zone with HP values of 2–6 μW m⁻³ (dark blue), while the central and southern portions exhibit elevated HP of 8–12 μW m⁻³ (yellow to light orange). A pronounced localized high occurs along the western edge where HP peaks at 16–18 μW m⁻³. The 3D Surface Model (Fig. 11b) emphasizes the topographic contrast between the northern "radiometric trough" and the southern "heat plateau." The western high manifests as a distinct vertical ridge, clearly rising above the surrounding surface. Generally, the R3 surface is relatively coherent and exhibits large-scale structural features, in contrast to the irregular, "noisy" surfaces of other sedimentary units, explaining its superior statistical performance. The geological implications suggest that the observed HP patterns are structurally controlled. The latitudinal banding and prominent western ridge likely reflect the influence of underlying basement structures or faults aligned with regional NE–SW and E–W magnetic trends.

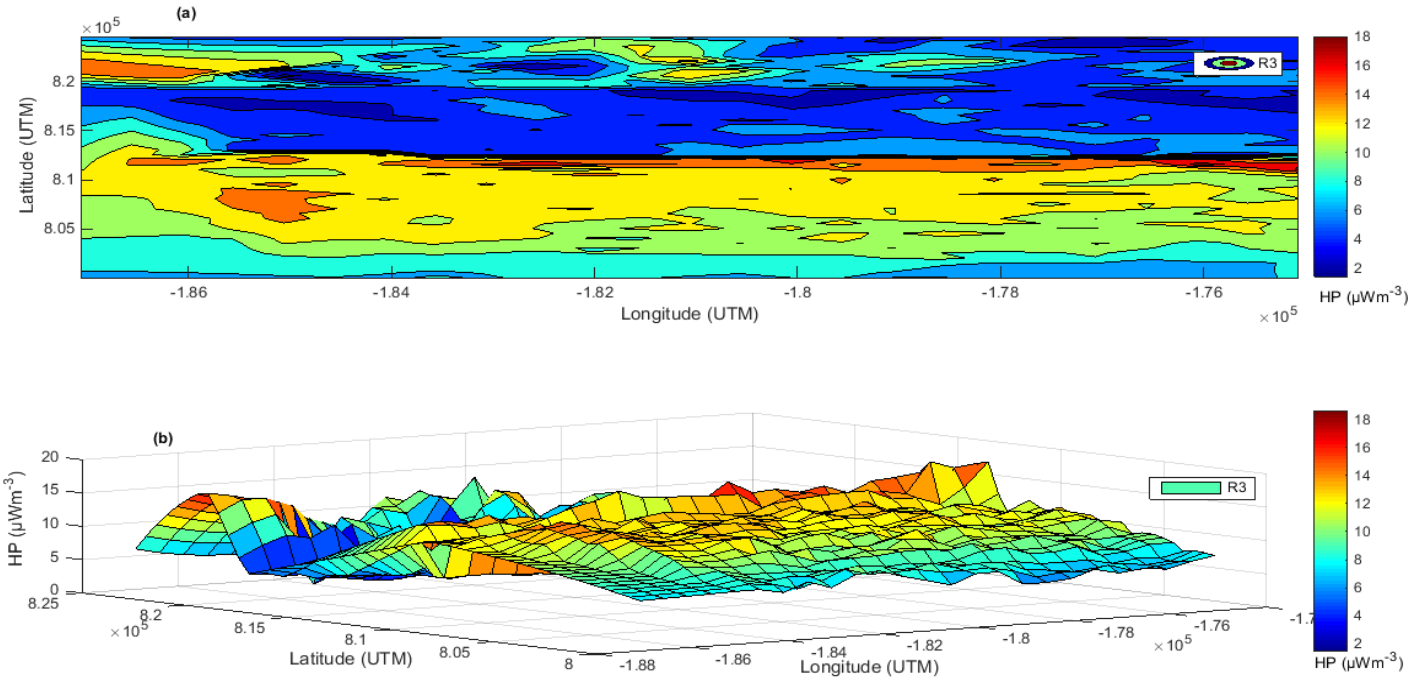

Fig. 11: Spatial representation of heat produced in (a) 2D contour (b) 3D Surface forms for R3 unit

3.4 Descriptive Statistics of Airborne Radiogenic Heat Parameters across Lithological Units

The statistical table summarizes the distribution of uranium- (HU, HGU), thorium- (HTh, HGT), potassium- (HK, HGK), and total radiogenic heat (TOTHP, TOTHG) across the ten lithological units (Table 2). The histogram was constructed to examine the geothermal distribution of heat produced across all the characterized lithological units (Fig.12). The radiogenic parameters exhibit wide spatial variability that reflects lithological composition, alteration processes, and source heterogeneity.

3.5 Basement Complex Units (A1–A4)

Unit A1 shows the widest range and highest extreme values among all lithologies. Uranium-derived heat (HU) varies from –0.31 to 15.61 μW m⁻³, with a mean of 4.09 μW m⁻³, while thorium-derived heat (HT) ranges from 0.31 to 59.64 μW m⁻³, averaging 7.13 μW m⁻³. Potassium heat contribution (HK) is relatively low, ranging between –0.07 and 1.61 μW m⁻³, with a mean of 0.20 μW m⁻³. Total heat produced (TOTHP) spans a very broad interval of 0.81–68.55 μW m⁻³, with a mean value of 11.42 μW m⁻³. Correspondingly, heat generated parameters show HU-equivalent values (HGU: –0.74–37.17 μW m⁻³, mean 9.74 μW m⁻³) and a maximum TOTHG of 163.22 μW m⁻³, with a mean of 27.20 μW m⁻³. These wide ranges and high means indicate intense but localized radiogenic enrichment within A1.

In A2, HU ranges from 0.22 to 8.34 μW m⁻³, with a mean of 2.53 μW m⁻³, while HT varies between 0.16 and 13.55 μW m⁻³, averaging 2.38 μW m⁻³. HK values remain modest (0.00–1.35 μW m⁻³, mean 0.29 μW m⁻³). TOTHP ranges from 0.97 to 21.51 μW m⁻³, with a mean of 5.20 μW m⁻³. The corresponding TOTHG values extend from 2.30 to 51.22 μW m⁻³, averaging 12.37 μW m⁻³. Compared with A1, A2 exhibits narrower ranges and lower mean values, suggesting more uniform radiogenic characteristics.

Unit A3 records HU values between 0.26 and 11.67 μW m⁻³, with a mean of 2.95 μW m⁻³, and HT values from 0.41 to 13.41 μW m⁻³, with a mean of 2.91 μW m⁻³. HK remains low (–0.03–1.44 μW m⁻³, mean 0.35 μW m⁻³). TOTHP varies from 1.25 to 23.94 μW m⁻³, with a mean of 6.22 μW m⁻³, while TOTHG spans 2.97–57.01 μW m⁻³, averaging 14.80 μW m⁻³. These values indicate moderate radiogenic heat production with occasional high anomalies.

A4 displays consistently high mean radiogenic values. HU ranges from 0.64 to 19.74 μW m⁻³, with a mean of 7.26 μW m⁻³, while HT varies between 1.30 and 15.68 μW m⁻³, averaging 5.12 μW m⁻³. HK shows a limited range (–0.04–1.50 μW m⁻³, mean 0.15 μW m⁻³). TOTHP ranges from 3.31 to 26.90 μW m⁻³, with a mean of 12.53 μW m⁻³, and TOTHG varies from 7.88 to 64.04 μW m⁻³, averaging 29.84 μW m⁻³—the highest mean among all lithological units.

Units A1–A4, mapped dominantly over migmatite, granite gneiss, biotite granite, porphyritic granite, and granodiorite terrains, exhibit the highest HP values and widest distribution ranges. The histogram for A1, which spatially coincides with felsic granitoids and migmatitic rocks, shows strong positive skewness with a long high-HP tail (Figure Fig. 12a). This reflects localized enrichment of uranium and thorium typical of evolved felsic basement rocks. A2, mapped largely over quartzite schist and less radiogenically enriched basement lithologies, displays a narrower and lower-centered unimodal HP distribution (Fig. 12b), indicating relatively homogeneous radiogenic content. A3**,** associated with mixed basement assemblages (migmatite–gneiss–schist), exhibits moderate variability and right-skewed distributions (Figure Fig. 12c), consistent with heterogeneous mineralogical composition. A4, which covers a broad area of migmatitic and biotite-rich basement rocks, shows a broader and weakly bimodal distribution (Figure 12d), suggesting internal compositional contrasts and interlayering of radiogenically enriched and depleted rocks. Collectively, the histogram patterns validate the classification of A-units as crystalline basement terrains with strong lithological control on HP. Generally, the heat produced in basement unit are found to be of economic interest since the estimated mean heats produced are higher than 4.0 μW m⁻³ IAEA (2003) recommended limit.

3.6 Weathered Basement Units (W1–W3)

In unit W1, HU values range from 0.30 to 7.54 μW m⁻³, with a mean of 2.48 μW m⁻³, while HT spans 0.54–33.28 μW m⁻³, with an average value of 4.18 μW m⁻³. HK remains low (–0.02–0.28 μW m⁻³, mean 0.03 μW m⁻³). TOTHP varies from 1.05 to 36.50 μW m⁻³, with a mean of 6.69 μW m⁻³, whereas TOTHG ranges from 2.51 to 86.91 μW m⁻³, with a mean of 15.92 μW m⁻³. In W2, HU ranges from 0.12 to 8.10 μW m⁻³, with a mean of 1.56 μW m⁻³, and HT ranges between 0.15 and 4.05 μW m⁻³, averaging 1.52 μW m⁻³. HK varies from

–0.01 to 0.75 μW m⁻³, with a mean of 0.10 μW m⁻³. TOTHP spans 0.50–11.14 μW m⁻³, with a mean of 3.18 μW m⁻³, while TOTHG ranges from 1.19 to 26.52 μW m⁻³, averaging 7.57 μW m⁻³, indicating comparatively lower heat output.

Unit W3, HU values vary between *–0.55 and 5.50 μW m⁻³*, with a mean of *2.08 μW m⁻³*, while HT spans *–0.09–12.17 μW m⁻³*, averaging *2.67 μW m⁻³*. HK ranges from *0.01 to 1.29 μW m⁻³*, with a mean of *0.31 μW m⁻³*. TOTHP varies from *–0.35 to 15.51 μW m⁻³*, with a mean of *5.06 μW m⁻³*, and TOTHG from *–0.84 to 36.94 μW m⁻³*, with a mean of *12.04 μW m⁻³*.

The weathered basement units (W1–W3) occur as transitional zones overlying the basement complex, mapped over deeply weathered granites, gneisses, and schists. Their histogram distributions show lower HP magnitudes and reduced variability compared to the fresh basement units, highlighting the modifying effect of chemical weathering. The distribution of W1, developed over heterogeneous basement rocks, exhibits right-skewed HP distributions with low modal values but extended tails, indicating residual concentration of radiogenic minerals during weathering (Fig. 12e). W2, spatially associated with intensely weathered profiles, shows the lowest and most compact HP distribution (Fig. 12f), reflecting strong leaching and depletion of heat-producing elements. W3, mapped over mixed weathered schist and gneiss units, displays broader and more symmetric HP distributions (Fig. 12g), suggesting partial retention and redistribution of radiogenic minerals. These patterns confirm that weathering attenuates radiogenic heat production while preserving lithological inheritance. The mean heat produced in two of the lithological units (W1and W3) in weathered basement terrain are above the IAEA (2003) recommended limit except W2 whose value falls below the limit.

3.7 Sedimentary Units (R1–R3)

In the R1 unit, HU ranges from –0.14 to 5.45 μW m⁻³, with a mean of 1.76 μW m⁻³, while HT varies between –0.23 and 5.32 μW m⁻³, with average value of 1.85 μW m⁻³. HK values are very low (–0.04–0.32 μW m⁻³, mean 0.02 μW m⁻³). TOTHP ranges from –0.08 to 8.85 μW m⁻³, with a mean of 3.63 μW m⁻³, while TOTHG varies between –0.20 and 21.08 μW m⁻³, averaging 8.64 μW m⁻³. R2 unit shows HU values between –0.62 and 4.56 μW m⁻³, with a mean of 2.11 μW m⁻³, and HT from –0.48 to 5.22 μW m⁻³, averaging 2.49 μW m⁻³. HK values range from –0.04 to 0.51 μW m⁻³, with a mean of 0.09 μW m⁻³. TOTHP spans within –0.74–9.66 μW m⁻³, with a mean value of 4.69 μW m⁻³, while TOTHG ranges from –1.76 to 23.00 μW m⁻³, averaging 11.17 μW m⁻³.

Unit R3 records HU values from –0.90 to 14.28 μW m⁻³, with a mean of 5.64 μW m⁻³, and HT values between 0.58 and 7.30 μW m⁻³, averaging 3.17 μW m⁻³. HK values range from –0.04 to 0.81 μW m⁻³, with a mean of 0.08 μW m⁻³. TOTHP varies from 1.25 to 19.85 μW m⁻³, with a mean of 8.89 μW m⁻³, while TOTHG spans 2.99–47.26 μW m⁻³, averaging 21.16 μW m⁻³, making R3 the most radiogenically enriched sedimentary unit.

The sedimentary units R1–R3, mapped over coastal plain sands, shale–limestone sequences, alluvium, and sand–clay–shale assemblages, show HP distributions primarily controlled by sediment provenance and depositional mixing**.** R1 exhibits flattened to weakly bimodal histograms (Fig. 12h), indicating sediments derived from multiple basement sources with contrasting radiogenic signatures. R2 shows a relatively symmetric unimodal distribution (Fig. 12i) centered on moderate HP values, consistent with well-mixed sedimentary deposits and uniform source contributions. In contrast, R3, mapped over mixed coastal and continental sediments, displays pronounced bimodality (Fig. 12j) with distinct low- and high-HP peaks, reflecting strong provenance heterogeneity and inheritance from both radiogenically enriched granitic basement and depleted schistose sources. These histogram characteristics reinforce the sedimentary classification and highlight the indirect lithological control on HP through source-rock contributions.

Table 2: The airborne statistical summary of heat produced and heat generated across the ten lithological zones

A1								
	HU	HT	HK	TOTHP	HGU	HGT	HGK	TOTHG
min	-0.31	0.31	-0.07	0.81	-0.74	0.75	-0.17	1.92
max	15.61	59.64	1.61	68.55	37.17	141.99	3.85	163.22
mean	4.09	7.13	0.20	**11.42**	9.74	16.98	0.48	27.20
stdv	2.34	6.89	0.28	8.55	5.58	16.40	0.66	20.37
kurt	1.07	5.31	3.61	3.52	1.07	5.31	3.61	3.52
skew	1.07	1.91	1.91	1.63	1.07	1.91	1.91	1.63
CV	57.27	96.57	139.73	74.90	57.27	96.57	139.73	74.90

W2								
	HU	HT	HK	TOTHP	HGU	HGT	HGK	TOTHG
min	0.12	0.15	-0.01	0.50	0.28	0.35	-0.02	1.19
max	8.10	4.05	0.75	11.14	19.28	9.64	1.78	26.52
mean	1.56	1.52	0.10	**3.18**	3.71	3.61	0.25	7.57
stdv	0.89	0.71	0.08	1.49	2.13	1.69	0.20	3.54
kurt	6.57	-0.52	5.16	2.21	6.57	-0.52	5.16	2.21
skew	2.11	0.45	1.75	1.29	2.11	0.45	1.75	1.29
CV	57.31	46.75	79.39	46.81	57.31	46.75	79.39	46.81

A2								
	HU	HT	HK	TOTHP	HGU	HGT	HGK	TOTHG
min	0.22	0.16	0.00	0.97	0.52	0.38	0.00	2.30
max	8.34	13.55	1.35	21.51	19.86	32.27	3.21	51.22
mean	2.53	2.38	0.29	**5.20**	6.02	5.66	0.69	12.37
stdv	1.37	1.64	0.18	2.80	3.25	3.91	0.43	6.66
kurt	1.91	4.75	1.68	2.80	1.91	4.75	1.68	2.80
skew	1.48	2.00	1.03	1.71	1.48	2.00	1.03	1.71
CV	54.02	69.14	61.45	53.83	54.02	69.14	61.45	53.83

W3								
	HU	HT	HK	TOTHP	HGU	HGT	HGK	TOTHG
min	-0.55	-0.09	0.01	-0.35	-1.30	-0.22	0.02	-0.84
max	5.50	12.17	1.29	15.51	13.11	28.97	3.08	36.94
mean	2.08	2.67	0.31	**5.06**	4.96	6.35	0.74	12.04
stdv	0.89	1.09	0.26	1.72	2.13	2.59	0.62	4.10
kurt	-0.15	4.04	0.47	0.67	-0.15	4.04	0.47	0.67
skew	0.17	0.81	1.21	0.18	0.17	0.81	1.21	0.18
CV	42.93	40.88	83.51	34.03	42.93	40.88	83.51	34.03

A3

	HU	HT	HK	TOTHP	HGU	HGT	HGK	TOTHG
min	0.26	0.41	-0.03	1.25	0.62	0.98	-0.06	2.97
max	11.67	13.41	1.44	23.94	27.78	31.93	3.42	57.01
mean	2.95	2.91	0.35	**6.22**	7.03	6.93	0.84	14.80
stdv	1.66	1.71	0.28	3.25	3.95	4.06	0.67	7.74
kurt	1.44	3.15	0.69	2.24	1.44	3.15	0.69	2.24
skew	1.36	1.55	1.17	1.47	1.36	1.55	1.17	1.47
CV	56.12	58.68	79.05	52.32	56.12	58.68	79.05	52.32

R1

	HU	HT	HK	TOTHP	HGU	HGT	HGK	TOTHG
min	-0.14	-0.23	-0.04	-0.08	-0.34	-0.55	-0.09	-0.20
max	5.45	5.32	0.32	8.85	12.97	12.66	0.75	21.08
mean	1.76	1.85	0.02	**3.63**	4.18	4.41	0.05	8.64
stdv	0.87	1.00	0.03	1.67	2.06	2.39	0.07	3.98
kurt	0.14	-0.31	8.13	-0.61	0.14	-0.31	8.13	-0.61
skew	0.62	0.53	2.36	0.41	0.62	0.53	2.36	0.41
CV	49.29	54.23	143.19	46.10	49.29	54.23	143.19	46.10

A4

	HU	HT	HK	TOTHP	HGU	HGT	HGK	TOTHG
min	0.64	1.30	-0.04	3.31	1.52	3.09	-0.11	7.88
max	19.74	15.68	1.50	26.90	46.99	37.33	3.57	64.04
mean	7.26	5.12	0.15	**12.53**	17.29	12.18	0.37	29.84
stdv	3.34	1.31	0.23	4.15	7.95	3.11	0.55	9.89
kurt	-0.03	2.01	4.42	-0.37	-0.03	2.01	4.42	-0.37
skew	0.80	0.27	1.98	0.48	0.80	0.27	1.98	0.48
CV	45.96	25.57	148.89	33.14	45.96	25.57	148.89	33.14

R2

	HU	HT	HK	TOTHP	HGU	HGT	HGK	TOTHG
min	-0.62	-0.48	-0.04	-0.74	-1.47	-1.14	-0.09	-1.76
max	4.56	5.22	0.51	9.66	10.85	12.43	1.22	23.00
mean	2.11	2.49	0.09	**4.69**	5.03	5.93	0.21	11.17
stdv	0.73	0.95	0.10	1.60	1.73	2.26	0.23	3.80
kurt	0.75	0.72	2.03	0.96	0.75	0.72	2.03	0.96
skew	-0.31	-0.66	1.67	-0.57	-0.31	-0.66	1.67	-0.57
CV	34.47	38.19	109.27	34.07	34.47	38.19	109.27	34.07

	W1									R3							
	HU	HT	HK	TOTHP	HGU	HGT	HGK	TOTHG		HU	HT	HK	TOTHP	HGU	HGT	HGK	TOTHG
min	0.30	0.54	-0.02	1.05	0.72	1.27	-0.05	2.51	min	-0.90	0.58	-0.04	1.25	-2.14	1.37	-0.10	2.99
max	7.54	33.28	0.28	36.50	17.95	79.25	0.67	86.91	max	14.28	7.30	0.81	19.85	33.99	17.39	1.94	47.26
mean	2.48	4.18	0.03	**6.69**	5.90	9.95	0.07	15.92	mean	5.64	3.17	0.08	**8.89**	13.42	7.55	0.19	21.16
stdv	0.99	3.48	0.03	3.97	2.35	8.28	0.06	9.46	stdv	2.49	1.29	0.09	3.66	5.92	3.07	0.22	8.72
kurt	1.09	7.04	5.41	5.29	1.09	7.04	5.41	5.29	kurt	-1.12	-1.05	11.91	-1.27	-1.12	-1.05	11.91	-1.27
skew	0.89	2.33	1.88	2.01	0.89	2.33	1.88	2.01	skew	0.09	0.14	2.70	0.13	0.09	0.14	2.70	0.13
CV	39.78	83.18	90.55	59.42	39.78	83.18	90.55	59.42	CV	44.11	40.71	111.86	41.20	44.11	40.71	111.86	41.20

Min -Minimum, Max – Maximum, Stdv – Standard deviation, Kurt – Kurtosis, Skew – Skewness, CV – Coefficient of variation.

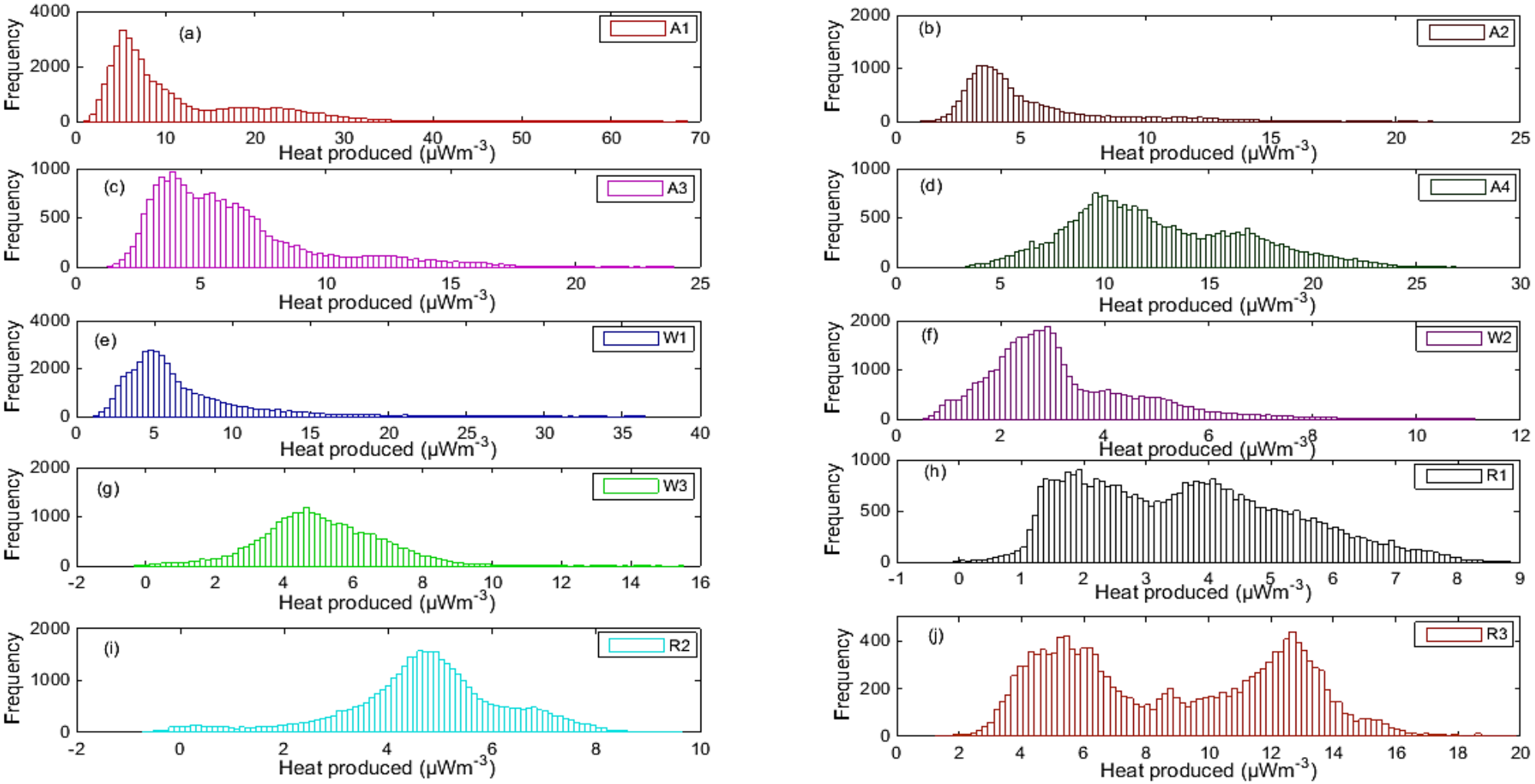

Fig. 12: Histogram representation of heat produced across the ten lithological units

3.8 Box-and-Whisker analysis of Heat Production across the Lithological Units

The box-and-whisker plot (Fig. 13) provides a robust statistical summary of the distribution of heat produced (HP) across the basement complex (A1–A4), weathered basement (W1–W3), and sedimentary units (R1–R3). The median, interquartile range (IQR), whisker extent, and outliers collectively reveal both the central tendency and anomalous radiogenic behavior associated with specific lithologies.

3.9 Basement Complex Units (A1–A4)

In A1 unit (Fig.13), the lithospheric response exhibits the widest spread and highest frequency of extreme outliers**,** with HP values extending well beyond the upper whisker to approximately 65–70 μW m^{-3}**.** The large IQR and elongated upper whisker indicate strong heterogeneity and multiple anomalous sources**,** consistent with localized enrichment of radiogenic minerals. This behavior spatially coincides with porphyritic granite, fine-grained biotite granite, migmatite, and granodiorite units on the geological map. These lithologies are characteristically enriched in uranium (U), thorium (Th), and potassium (K) due to the presence of K-feldspar, biotite, muscovite, and accessory phases such as zircon and monazite. The median lies well above those of most other units, highlighting A1 as a dominant heat-producing basement domain. A2 unit (Fig. 13) displays a narrower IQR and comparatively fewer outliers, although several moderate upper outliers (18–22 μW m^{-3}) are present. The tight clustering of the central box suggests relatively uniform heat production, with anomalies likely reflecting localized lithological inclusions rather than pervasive enrichment.

In A3 unit, a moderate IQR and a concentration of upper outliers between 20 and 25 μW m^{-3} was experienced (Fig. 13)**.** The presence of these outliers, coupled with a median higher than A2 but lower than A4, implies intermediate radiogenic enrichment**,** possibly controlled by mixed lithologies or partial granitoid influence. Units A2 and A3 show moderate medians and fewer extreme outliers due to the gneiss, amphibolite schist, quartzite schist, and mixed granitoid–schist assemblages. These lithologies contain lower proportions of K-rich and U–Th-bearing minerals relative to granites, resulting in intermediate heat-production levels with localized anomalies where felsic intrusions or metasomatic enrichment occur A4 unit **is** characterized by a high median HP and a broad upper whisker, with several pronounced outliers approaching 25–27 μW m^{-3}**.** The compact lower quartile and extended upper tail indicate that while background heat production is consistently high, localized anomalous zones contribute significantly to the overall heat budget. The result obtained in the basement group is in accordance with that of Furlong & Chapman (2013), Hasterok *et al.* (2018), Artemieva & Mooney (2001) and Karg *et al.* (2024),

3.10 Weathered Basement Units (W1–W3)

Unit W1, which records the most prominent anomalies within the weathered basement (large number of upper outliers, extending to approximately 35–37 μW m^{-3}), overlies deeply weathered granitic and migmatitic basement rocks (Figure 13)**.** On the geological map, W1 corresponds to areas adjacent to basement granites and gneisses where chemical weathering concentrates immobile U- and Th-bearing minerals in the regolith, while K may be partially retained in clay minerals. The skewed distribution and elongated upper tail indicate that weathering processes have concentrated radiogenic elements, producing localized but intense heat anomalies relative to the bulk population. Unit W2, characterized by the lowest median and minimal outliers, corresponds to weathered shale, limestone, and sand–clay sequences. These lithologies are inherently poor in radiogenic elements and are further depleted by leaching during weathering, producing a statistically compact and subdued heat-production signature. Unit W3 shows moderate medians with both upper and lower outliers and is spatially associated with mixed

weathered basement and sedimentary contacts. The variable heat response reflects heterogeneous regolith development, where localized basement influence enhances heat production while extensive sediment cover suppresses it elsewhere (Wilford *et al.*, 1997; Airo, 2002; Hasterok and Chapman, 2011; Vargas *et al.*, 2022)

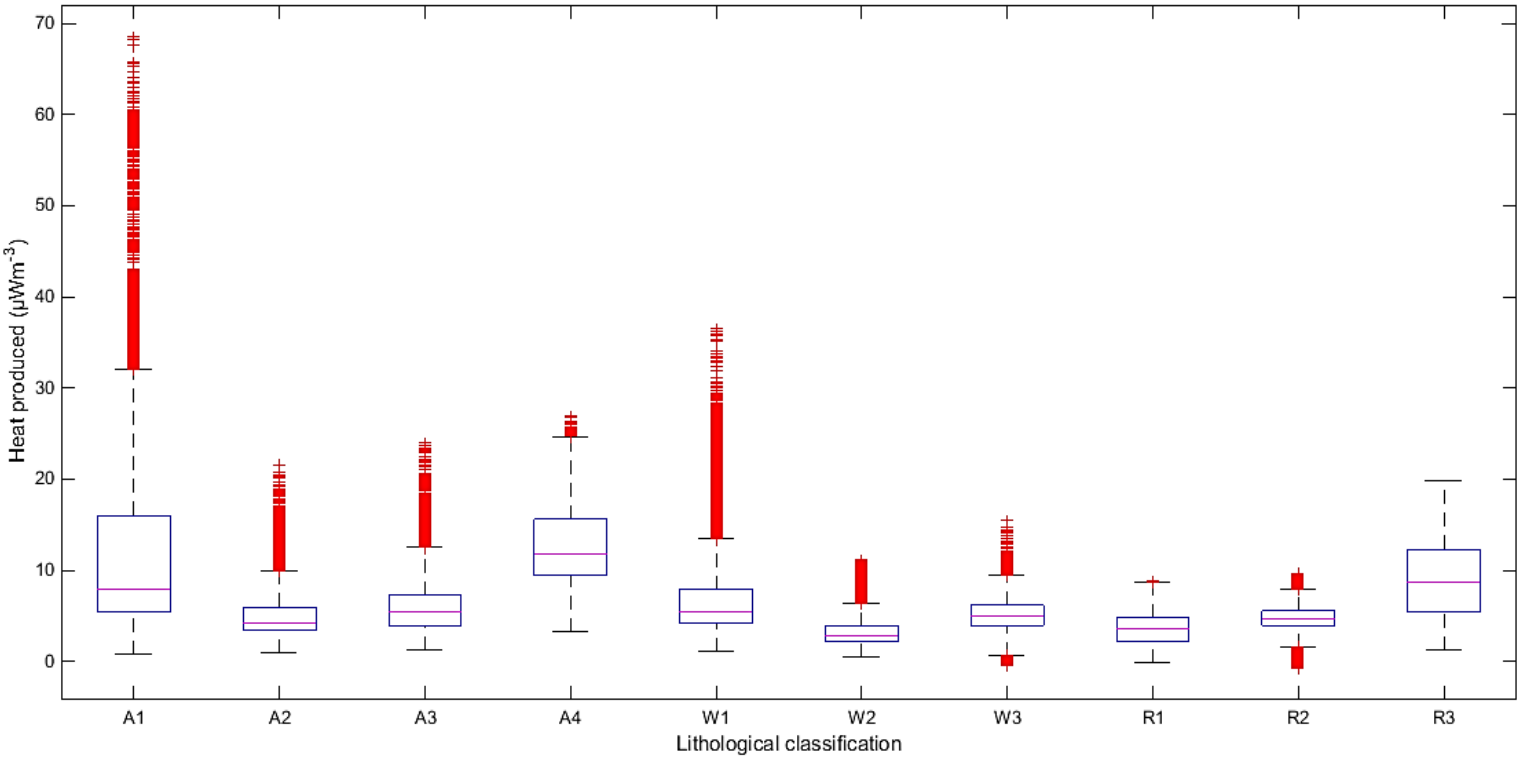

Fig. 13: Box and Whisker plot representation showing the geothermal outlier for heat produced across the ten Lithological units.

Unit R1, displaying low medians and narrow IQRs, corresponds to coastal plain sands, shale, limestone, and recent alluvium. These sedimentary rocks are dominantly quartz-rich and carbonate-rich, with minimal U–Th–K content, explaining the uniform and low heat-production values. Unit R2, which shows slightly higher variability and occasional anomalies, maps onto sandstone–limestone interbeds and Ewekoro Formation units**.** Unit R2 displays a similar central tendency to R1 but with slightly more variability and both upper and lower outliers. The negative lower outliers indicate minimal radiogenic contribution, while occasional upper anomalies (8–10 μW m^{-3}) suggest localized basement influence. Unit R3 was found to stands out among the sedimentary units with elevated medians and upper outliers extending to 18–20 μW m^{-3}. Geologically, R3 coincides with sandstone units proximal to basement outcrops and structurally controlled boundaries, where sedimentary rocks inherit radiogenic minerals from adjacent granitic and gneissic sources. This basement inheritance accounts for the anomalously high heat production relative to other sedimentary units.

Generally, the box-and-whisker plot reveals a systematic decrease in both median heat production and anomaly magnitude from basement to sedimentary terrains. The most pronounced anomalies occur in A1, A4, and W1, where extreme upper outliers indicate proximal or concentrated radiogenic sources**.** In contrast, W2, R1, and R2 show subdued variability, reflecting diffuse or depleted heat sources. The asymmetry of most distributions, marked by extended upper tails, suggests that radiogenic heat production is dominated by localized enrichment rather than uniform background processes**.** These anomalous responses corroborate earlier histogram patterns and inferential statistical results, reinforcing the role of lithology and alteration history in controlling spatial heat variability.

The anomalous heat-production signatures observed in the box-and-whisker analysis can be directly correlated with the spatial distribution and mineralogical composition of rock types mapped within the basement complex, weathered basement, and sedimentary terrains. The spatial correspondence between statistical anomalies and mapped lithologies confirms that radiogenic heat production is fundamentally controlled by lithology and mineralogy (Rudnick *et al*., 1998; Vila *et al.,* 2010). The granitic and migmatitic basement rocks therefore act as primary heat sources, weathered equivalents serving as secondary concentrators, and sedimentary units reflecting varying degrees of dilution or basement inheritance. The strongest anomalies (A1, A4, W1, and R3) consistently align with felsic, K-rich, and U–Th-enriched rock types, validating the geological map as a critical framework for interpreting heat-production variability.

3.12 Meteorological modeling with heat produced

Figures 14 - 16 focused on the temporal (quasi-spectral) variation of Radiogenic Heat Production (HP), Relative Humidity (RH), and Surface Temperature (Temp) over the basement, weathered basement and sedimentary terrains for two lithological units, Station I and Station II, respectively**.** Although the data are plotted in the time domain, the signals exhibit clear quasi-cyclic, spectral-like patterns that reflect the interaction between atmospheric forcing (temperature and humidity) and lithospheric radiogenic heat contributions.

3.13 Spatial and temporal variations of radiogenic heat, relative humidity, and surface temperature in basement terrains

In the Station I of basement unit (Fig. 14a), radiogenic heat production (HP) exhibits moderate variability throughout the monitoring period, with pronounced

fluctuations around days 50, 100, and 200. These episodic changes suggest that HP is highly sensitive to local lithological variations or transient changes in moisture content. Relative humidity (RH) displays inverse trends with HP in several intervals, particularly between days 50–150 and 250–350, indicating that increased moisture may suppress heat dissipation or alter the thermal conductivity of near-surface materials. Surface temperature (Temp) remains relatively stable at 21–22 °C during the early monitoring period but gradually decreases after day 150, suggesting a slow cooling trend potentially associated with seasonal changes or cumulative diurnal effects influencing surface heat exchange.

In contrast, Station II of basement unit (Fig. 14b) shows generally lower HP values, fluctuating mostly between 10–40 $\mu W\ m^{-3}$, which reflects spatial variability in radiogenic element distribution or differences in basement rock composition. RH at this station remains higher and more stable, averaging around 35–45%, with less pronounced fluctuations compared to Station I. Temperature trends demonstrate a gradual decline from approximately 35 °C to 28 °C, punctuated by minor peaks that may reflect short-term warming events. Interestingly, HP peaks at Station II often coincide with small drops in RH, implying a coupling between local moisture levels and radiogenic heat output.

When considered together, the spectral variations across both stations reveal several key insights. HP is highly dynamic and closely linked to local lithological and environmental conditions. RH and HP show occasional inverse relationships, suggesting that moisture content significantly influences near-surface heat flux. While temperature trends are generally smoother than those of HP or RH, they still capture seasonal or diurnal thermal variations that can modulate surface radiogenic heat dissipation. Station I is higher HP variability likely reflects more radiogenically enriched lithologies or the influence of shallower weathered basement rocks, whereas Station II's lower HP and more stable RH indicate a more homogeneous basement environment. Overall, these spectral patterns demonstrate that radiogenic heat production in basement terrains is governed by an interplay of intrinsic lithological properties and extrinsic environmental factors such as surface moisture and temperature.

3.14 Spatial and temporal variations of radiogenic heat, relative humidity, and surface temperature in weathered basement terrain

At Station I (Fig. 15a), the radiogenic heat production (HP, red line) displays moderate but distinct fluctuations throughout the monitoring period. Several peaks and troughs suggest that HP is highly sensitive to the local lithological variability and transient environmental factors, such as moisture content within the weathered basement. The episodic nature of these peaks likely reflects zones enriched in radiogenic elements or localized changes in thermal conductivity due to moisture infiltration. Relative humidity (RH, blue line) at this station remains relatively stable but occasionally exhibits inverse trends with HP, particularly during sharp HP peaks. This inverse relationship suggests that increased soil moisture may temporarily dampen radiogenic heat flux, either by enhancing near-surface thermal conductivity or by acting as a heat

sink. Surface temperature (Temp, yellow line) is initially steady at 21–22 °C but shows a gradual decline after day 150, reflecting slow seasonal cooling or cumulative diurnal effects. This decreasing temperature trend may subtly reduce the surface thermal gradient, influencing the dissipation of HP from the subsurface.

In contrast, Station II (Fig. 15b) exhibits lower HP magnitudes, generally oscillating between 5–15 $\mu W\ m^{-3}$, with reduced temporal variability. This pattern indicates a more homogeneous basement composition or lower concentrations of radiogenic elements. RH (blue line) begins at relatively high values (~100 %) and gradually decreases over the monitoring period, displaying a smoother trend compared to Station I. Minor peaks in HP correspond to slight drops in RH, suggesting that decreased moisture content allows more efficient radiogenic heat dissipation. Surface temperature (Temp, yellow line) increases steadily from around 20 °C to 32 °C, reflecting seasonal warming and accumulation of heat at the surface, which likely reinforces the thermal gradient driving heat flux from the basement.

Across both stations, radiogenic heat production (HP) exhibits pronounced variability that reflects both intrinsic lithological properties and environmental conditions. Station I displays higher HP fluctuations, likely resulting from heterogeneous lithologies and shallower weathered layers, whereas Station II shows lower and more stable HP trends, indicative of a more uniform basement composition. The coupling between HP and relative humidity (RH) is more pronounced at Station I, where increased moisture appears to suppress heat output, while at Station II this relationship is weaker due to relatively stable humidity levels. Surface temperature, although smoother than HP or RH, plays a significant role in modulating heat flux by influencing the thermal gradient between the weathered basement and the atmosphere; the gradual warming at Station II enhances heat dissipation, whereas the slight cooling at Station I may reduce it.

The spectral patterns observed at Stations I and II suggest that radiogenic heat production in weathered basement terrains is controlled by a combination of lithological heterogeneity, moisture dynamics, and surface temperature variations. Station-specific differences in HP magnitude and variability emphasize the importance of local lithological and hydrological conditions, while temperature and humidity collectively modulate the temporal distribution of subsurface heat flux.

3.15 Spatial and temporal variations of radiogenic heat, relative humidity, and surface temperature in sedimentary terrains

At Station I (Fig.16a), heat production (HP) shows moderate to high variability throughout the monitoring period, with recurrent peaks and troughs that indicate dynamic radiogenic heat behavior within the sedimentary sequence. These fluctuations likely reflect variations in sediment composition, such as alternating clay-rich and sandy units, which differ in their radiogenic element content. Relative humidity (RH) remains comparatively low and stable, showing only subtle changes over time. However, short-term inverse responses between HP and RH are evident, suggesting that increased moisture within the sediments may reduce effective heat transfer or attenuate near-surface radiogenic heat signals. The surface temperature (Temp) exhibits a gradual decline from about 32–33 °C to approximately 29 °C

toward the later part of the observation period. This smooth downward trend points to seasonal cooling and gradual atmospheric control rather than abrupt surface disturbances. The relatively smooth temperature variation compared to HP emphasizes that HP is more strongly influenced by subsurface sediment heterogeneity than by surface thermal conditions alone.

In Station II (Fig. 16b), HP values are generally lower and exhibit reduced variability compared to Station I, suggesting a more homogeneous sedimentary package with lower concentrations of heat-producing radioactive elements. The HP curve shows fewer sharp peaks, indicating relatively uniform radiogenic contributions from the subsurface**.** Relative humidity begins at higher values and decreases gradually with time, reflecting progressive drying of the sedimentary column or seasonal moisture redistribution. Minor HP peaks tend to coincide with local reductions in RH, implying that drier sediment conditions may enhance heat transmission to the surface. The temperature profile at Station II is notably higher than at Station I, ranging between 36 – 39 °C, and shows pronounced fluctuations with distinct warming and cooling phases. These variations suggest stronger atmospheric influence, possibly due to reduced vegetation cover or higher thermal conductivity of the sedimentary materials, which allows surface temperatures to respond rapidly to environmental forcing.

Across both sedimentary stations, HP exhibits greater short-term variability than RH or Temp, underscoring the dominant role of sediment composition and radiogenic element distribution in controlling heat production. RH generally shows an inverse or weak coupling with HP, highlighting the moderating effect of moisture on near-surface heat flux. Temperature trends are smoother and largely seasonal but can modulate the expression of radiogenic heat at the surface. Station I demonstrates stronger HP variability, likely due to more heterogeneous sedimentary layering, while Station II reflects more uniform sediment composition and stronger atmospheric control on temperature. Generally, the observed patterns confirm that radiogenic heat production in sedimentary terrains is governed by a combination of lithological variability, moisture dynamics, and surface thermal conditions, with lithology exerting the primary control and environmental factors acting as secondary modulators.

Across the two sedimentary terrains, variations in the studied parameters can be explained by distinct controlling factors. Heat Production (HP) is primarily lithology-dependent, with shale-rich terrains exhibiting higher radiogenic heat production (RHP) than sandstone-dominated terrains, while depth-dependent variations may arise from local stratigraphic differences. In contrast, surface temperature (Temp) and relative humidity (RH) are largely governed by atmospheric and surface conditions, displaying strong inverse correlations over diurnal and seasonal cycles, with additional modulation by terrain-specific factors such as soil moisture, land cover, and albedo. The relationship between subsurface HP and surface climatic variables is minimal;

any observed influence of radiogenic heat on Temp or RH is indirect and mediated through shallow subsurface thermal effects, which are secondary to the dominant meteorological and environmental controls.

The direct influence of radiogenic HP on surface temperature and relative humidity is negligible, as the geothermal flux (0.05 – 0.1 W/m²) is small relative to solar energy input (~1000 W/m² at peak daytime). Radiogenic heat primarily contributes to the shallow subsurface thermal regime, influencing temperature gradients at depth rather than the atmospheric boundary layer.

Indirect effects, such as shallow conduction into surficial soils, may slightly modify near-surface temperature; however, these effects are generally overshadowed by meteorological forcing (Harrison & Chapman, 1993). Heat transfer occurs via conduction from the subsurface to the surface, and via radiation, convection, and conduction from the surface to the atmosphere. Consequently, any observed correlation between HP and surface climatic variables is likely indirect and secondary to environmental factors, including soil moisture, albedo, vegetation, and topography.

Conclusively, variations in radiogenic heat production across sedimentary terrains primarily affect subsurface thermal gradients, whereas surface temperature and humidity are overwhelmingly controlled by atmospheric and environmental factors. Understanding these distinctions is critical for interpreting heat flow, basin thermal evolution, and local environmental dynamics.

Fig. 14: Spectral variation of heat produced (HP), relative humidity (RH) and surface temperature (Temp) over two basement terrain

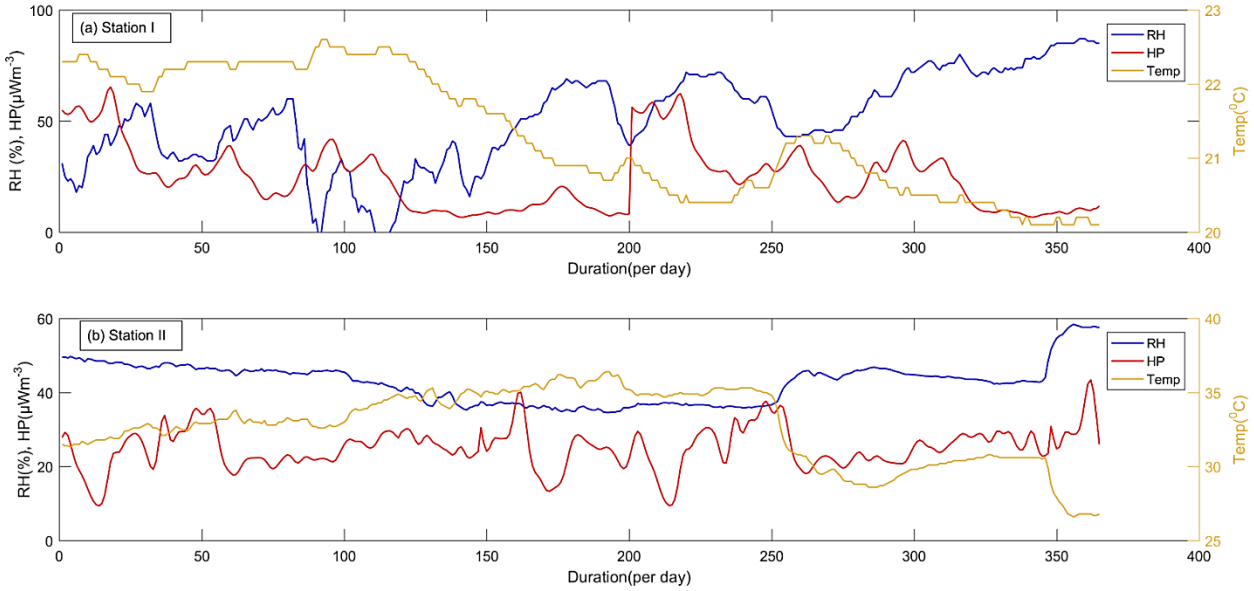

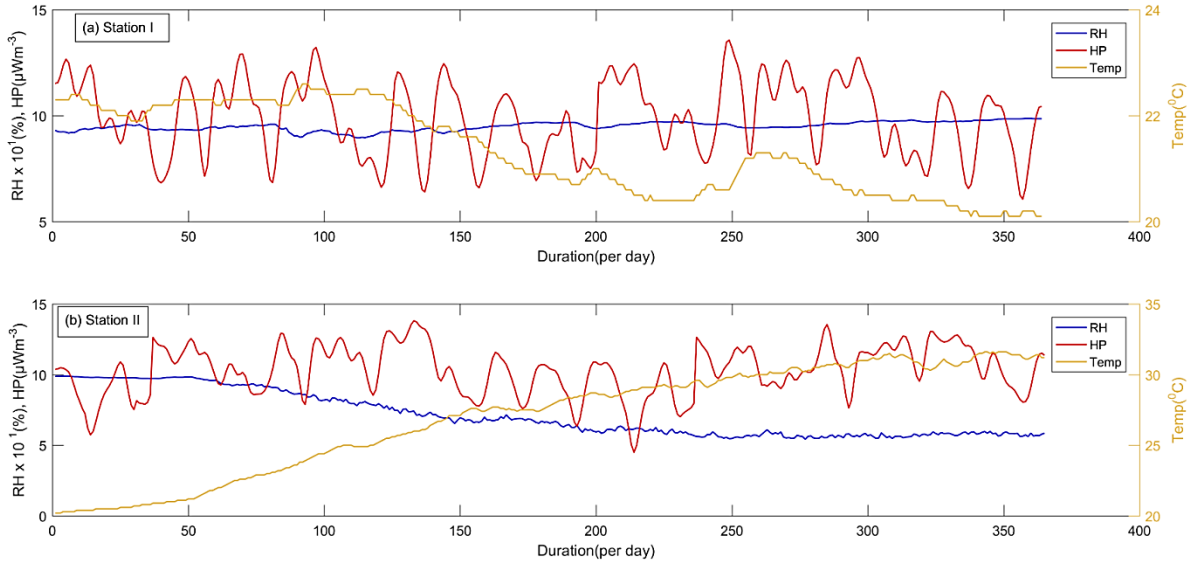

Fig. 15: Spectral variation of heat produced (HP), relative humidity (RH) and surface temperature (Temp) over two weathered basement terrain

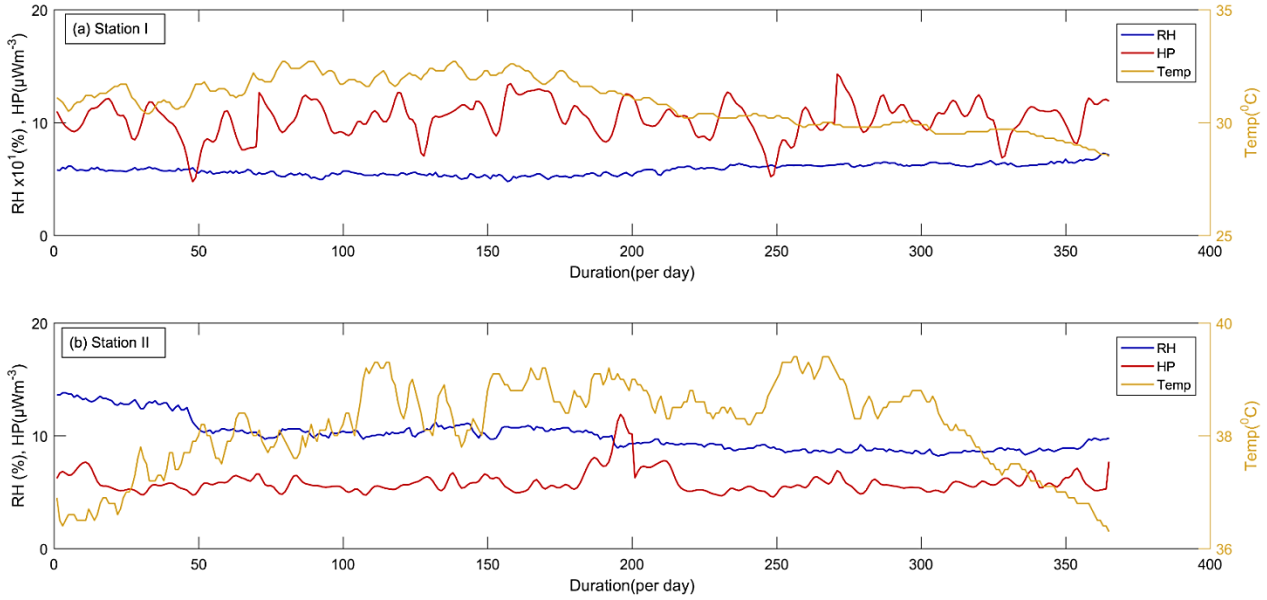

Fig. 16: Spectral variation of heat produced (HP), relative humidity (RH) and surface temperature (Temp) over two sedimentary terrain

3.16 Multiple Linear Regression Results across the Lithological Units

Multiple linear regression analysis was employed to establish the relationship between radiogenic heat production (HP) and the environmental variables temperature (T) and relative humidity (RH) across the basement, weathered basement, and sedimentary terrains**.** The regression performance was evaluated using the coefficient of determination (R^2) and F-statistics.

In the basement terrain (Table 3), the first regression model $HP = 2.55T - 0.05RH - 27.13$ shows a positive dependence of heat production on temperature and a weak negative influence of relative humidity. However, the low R^2 value (0.04) indicates that only 4% of the variability in HP is explained by T and RH. Despite this, the relatively higher F-value (8.02) suggests that the model captures a statistically meaningful trend, likely reflecting the thermally stable nature of crystalline basement rocks where temperature variations exert limited but observable influence on radiogenic heat.

The second model for the basement $HP = -0.04T + 0.04RH + 24.83$ exhibits negligible explanatory power ($R^2 = 0.002$; $F = 0.47$), indicating that neither temperature nor humidity significantly controls HP in this formulation. This suggests that radiogenic heat in the basement is predominantly governed by intrinsic lithological factors such as U, Th, and K content rather than ambient environmental conditions.

For the weathered basement (Table 3), both regression equations indicate negative relationships between HP and both temperature and relative humidity**:** $HP = -0.12T - 1.59RH + 27.59$ and $HP = -0.41T - 1.16RH + 29.78$. These models show modest but consistent R^2 values (0.02) and moderate F-statistics (3.98 and 3.05), implying limited explanatory power but improved sensitivity compared to the basement terrain. The stronger negative coefficients, particularly for RH, suggest that weathering processes, moisture infiltration, and element mobility significantly affect radiogenic heat production by promoting leaching or redistribution of radioactive elements in the regolith.

In the sedimentary terrain (Table 3), the first model $HP = 0.48T + 1.03RH - 9.98$ shows positive contributions from both temperature and humidity, with an R^2 of 0.04 and an F-value of 6.70. This indicates a weak but notable environmental control on HP, likely due to the influence of pore fluids, clay content, and moisture-dependent geochemical interactions common in sedimentary environments.

Conversely, the second sedimentary model $HP = 0.05T + 0.01RH + 3.82$ has very low explanatory power ($R^2 = 0.001$; $F = 0.22$), confirming that T and RH alone are insufficient to describe HP variability across all sedimentary settings. This highlights the dominant role of lithological heterogeneity and depositional processes in controlling radiogenic heat.

Across all lithological units, the low R^2 values indicate that temperature and relative humidity explain only a small fraction of the observed variability in radiogenic heat production. This underscores that HP is primarily controlled by geochemical composition and lithology, while environmental parameters exert only secondary modulation. The comparatively stronger model responses in the weathered basement and sedimentary terrains reflect increased sensitivity to surface and near-surface processes, whereas the fresh basement remains largely decoupled from atmospheric influences.

Table 3: Linear regression analysis of heat produced and the climatic parameters

Lithological Units	Regression Equation	R^2 - value	F -value
Basement	HP = 2.55T – 0.05 RH – 27.13	**0.04**	**8.02**
	HP = -0.04T +0.04 RH + 24.83	**0.002**	**0.47**
Weathered Basement	HP = -0.12T – 1.59 RH + 27.59	**0.02**	**3.98**
	HP = -0.41T – 1.16RH + 29.78	**0.02**	**3.05**
Sedimentary	HP = 0.48T + 1.03RH – 9.98	**0.04**	**6.70**
	HP = 0.05T + 0.01RH + 3.82	**0.001**	**0.22**

3.17 Statistical treatment of heat produced for proximal source analysis

In this study, the heats produced across the ten lithological units were subjected to inferential and multivariate statistical analysis to estimate the interrelationship among their sources. The inferential study utilizes two techniques; namely, F-test and T-test while the multivariate analysis adopted the usage of correlation analysis, principal component and cluster analysis.

3.18 Inferential Statistical Assessment of Proximal Heat Sources

The application of F-test and T-test in heat source proximate analysis enables the statistical evaluation of radiogenic heat variations among lithological units. The F-test assesses whether differences in heat production across multiple units are significant, while the T-test facilitates pairwise comparisons to identify specific units with distinct heat contributions. Together, these tests provide a rigorous framework for identifying and ranking dominant heat-producing lithologies, which is essential for thermal modeling, geothermal assessment, and understanding subsurface heat distribution.

Inferential statistical analyses using the F-test and T-test (Table 4) were applied to evaluate similarities in the variance and mean of radiogenic heat production (HP) across the ten lithological units, with the objective of identifying potential common proximal heat sources. While the F-test assesses similarity in HP variability and reflects comparable lithological heterogeneity, the T-test evaluates similarity in mean HP values, indicating equivalent radiogenic heat contributions. The combined application of both tests provides a robust statistical basis for distinguishing shared versus distinct heat-generating sources.

The F-test results (Table 4) reveal that Unit A1 is statistically distinct, sharing no common source with any other unit. This isolation reflects its highly variable HP distribution and suggests a unique, radiogenically enriched basement source. In contrast, Units A2, A3, and A4 exhibit limited but meaningful

variance similarities, primarily among themselves and with selected weathered or sedimentary units, indicating partial lithological affinity within the basement complex. Among the weathered basement units, W1–W3 show increasing variance similarity with sedimentary units (R1–R3), reflecting the transitional nature of weathered profiles and the redistribution of radiogenic elements during weathering and erosion. Notably, R2 shares variance similarity with the largest number of units, highlighting strong sedimentary mixing and inheritance from multiple proximal sources.

The T-test results (Table 4) indicate broader connectivity among lithological units based on mean HP similarity. Again, A1 remains isolated, confirming its role as a distinct heat source. In contrast, A3 shares common mean HP values with nearly all units except A1 and A2, suggesting that it represents a regional baseline basement source influencing multiple lithological classes. Units W2 and W3 also exhibit extensive mean similarity with both basement and sedimentary units, emphasizing their role as intermediary reservoirs linking fresh basement heat sources to sedimentary deposits. Sedimentary units, particularly R1 and R3**,** show strong mean similarity with several basement and weathered units, confirming that their radiogenic heat signatures are largely inherited from source lithologies rather than generated in situ.

When considered jointly, the F-test and T-test results delineate a hierarchical framework of proximal heat sources. Units sharing both variance and mean similarity are inferred to originate from common heat sources, whereas those sharing only mean similarity likely derive from similar lithologies but have undergone different post-emplacement processes such as weathering or sediment sorting. The persistent statistical isolation of A1 identifies it as a distinct radiogenic end-member, while the widespread linkages of A3, W3, W2, and R1 highlight their significance as key contributors to regional heat production.

Generally, the inferential statistical analysis demonstrates that radiogenic heat production across the study area is systematically controlled by lithology, degree of alteration, and sediment provenance. The integrated use of F-test and T-test provides a statistically rigorous and geologically meaningful approach for identifying proximal heat sources within complex basement, weathered, and sedimentary terrains.

Table: 4 Summary of F-test and T-test heat sources proximate statistical analysis

F-test		T-test	
Lithological units	**Hypothesis Remark**	**Lithological units**	**Hypothesis Remark**
A1	Share no common source with any units	A1	Share no common source with any units
A2	Sources common in 3 units (A4, RI and R2)	A2	Share common sources with five units (A4, W1, W2, R1 and R3)
A3	Sources common in 3 units (A4, WI and W3)	A3	Share common source with all units except A1 and A2
A4	Share no common source with any units except A2 and A3	A4	Share no common source with any units except A2 and A3

W1	Sources common in 2 units (A3 and R2)	W1	Share common source with 4 units (A3, W3, R1 and R3)
W2	Share common source with 3 units (R1, R2 and R3)	W2	Share common sources with 5 units (A3, W3, R1, R2 and R3)
W3	Share common source with 4 units (A3, R1, R2 and R3)	W3	Share common source with 6 units (A2, A3, W1, W2, R1 and R3)
R1	Share common source with 4 units (A2, W2, W3 and R3)	R1	Share common source with 6 units (A2, A3, W1, W2, W3 and R3)
R2	Share common source with 5 units (A2, W1, W2, W3 and R3)	R2	Share common source with 3units (A3, W2 and R2)
R3	Share common source with 4 units (W2, W3, R1 and R2)	R3	Share common source with 5 units (A2, W1, W2, W3 and R1)

3.19

Multivariate statistical analysis

Multivariate statistical analysis provides a robust framework for examining complex relationships among multiple geophysical and geochemical parameters across diverse lithological units. In sedimentary and basement terrains, lithological heterogeneity often controls variations in radiogenic heat production, mineral composition, and associated geophysical properties. Analyzing these variations simultaneously allows for the identification of dominant factors, patterns of similarity or dissimilarity among units, and potential underlying geological controls.

In this study, adequacy of the dataset for factor analysis was assessed using the Kaiser–Meyer–Olkin (KMO) measure and Bartlett's test of sphericity. The KMO value of 0.654 indicates acceptable sampling adequacy, while Bartlett's test was highly significant (χ^2 = 21639.481, $p < 0.001$), confirming that the correlation matrix is not an identity matrix. These results demonstrate that the dataset is appropriate for factor analysis. The ten lithological units were subjected to multivariate statistical techniques, including Principal Component Analysis (PCA) and cluster analysis, to elucidate the primary controls on radiogenic heat production and to classify units based on their thermal and compositional characteristics. This approach enables a comprehensive understanding of the relationships among lithology, thermal behavior, and geophysical properties, which is essential for applications such as geothermal assessment, basin modeling, and resource exploration.

Principal Component Analysis (PCA) was applied to the radiogenic heat dataset to identify the dominant controls on heat production across the ten lithological units and to reduce the dimensionality of the multivariate dataset. Four principal components (PC1–PC4) with eigenvalues greater than unity were retained, collectively explaining 61.70% of the total variance (Table 5). Similar levels of explained variance (between 55–70%) have been reported in radiometric and geothermal PCA studies where multiple geological processes interact to control the spatial distribution of heat-producing elements (HPEs) such as U, Th, and K. Studies on airborne gamma-ray spectrometry datasets have shown that the

first few principal components commonly capture lithological composition, weathering processes, and secondary redistribution of radioelements (Vila *et al.*, 2010; Hasterok *et al*., 2018). The moderate cumulative variance observed in this study therefore reflects the multifactorial controls on radiogenic heat production, consistent with findings from other basement and mixed sedimentary terrains (Rudnick *et al*., 1998; Artemieva and Mooney, 2001; Salem and Ali 2015; Karg *et al.*, 2024).

Principal Component 1 (PC1) explains 23.23% of the total variance and represents the dominant lithological control on radiogenic heat production. Strong positive loadings in units R3 (0.733), W2 (0.567), A1 (0.553), and A4 (0.454) indicate lithologies enriched in heat-producing elements, while strong negative loadings in W3 (−0.681) and A3 (−0.519) correspond to comparatively depleted or altered units. Similar interpretations have been reported in crustal heat production studies where the first principal component typically reflects primary lithological composition and mineralogical enrichment of uranium, thorium, and potassium, particularly in felsic and pegmatitic rocks (Abbady and Ghamdi 2018; Hasterok and Webb, 2017). These elements are commonly hosted in accessory minerals such as zircon, monazite, and allanite, which are unevenly distributed across basement lithologies, leading to pronounced radiogenic contrasts.

Principal Component 2 (PC2), accounting for 16.32% of the variance, appears to reflect secondary redistribution processes, particularly weathering and sedimentary reworking. Positive loadings in R2 (0.664) and W2 (0.553) and negative loadings in A1 (−0.515) and R1 (−0.387) suggest that PC2 captures variations resulting from the mobility of uranium and potassium during weathering and fluid interaction. Previous studies have shown that weathering processes can significantly modify radiometric signatures by leaching or concentrating radioelements in weathered profiles and sedimentary environments (Wilford *et al*., 1997; Airo, 2002; Furlong and Chapman 2013; Rolandone 2013). As such, PC2 effectively distinguishes relatively stable basement units from more dynamic weathered and sedimentary terrains.

Principal Component 3 (PC3) explains 12.13% of the variance and is characterized by strong positive loadings in A2 (0.751) and A4 (0.585), with moderate influence from A3 (0.417). These loadings, predominantly associated with basement lithologies, suggest localized geological controls such as mineralogical heterogeneity, structural deformation, or fracture-controlled enrichment of heat-producing minerals. Similar PCA interpretations have been reported in crystalline basement studies where secondary components capture intra-basement variability linked to tectonic structures and localized magmatic differentiation (Rybach, 1988; Hasterok and Chapman, 2011; Vargas *et al*., 2022).

Principal Component 4 (PC4), accounting for 10.02% of the variance, is dominated by a strong loading in R1 (0.792), with secondary contributions from A3 (0.390) and R3 (0.221). This component likely represents sedimentary or diagenetic influences on radioelement distribution. In sedimentary basins, processes such as compaction, cementation, and clay mineral concentration can locally modify the distribution of uranium and thorium, producing distinct radiometric signatures separate from primary lithological controls (Markwick *et al*., 2021). The identification of PC4 therefore highlights the contribution of localized sedimentary processes to the overall radiogenic heat variability.

An integrated interpretation of the PCA results shows that the first two components (PC1 and PC2) together explain 39.55% of the total variance, indicating that lithological composition and weathering processes are the primary controls on radiogenic heat production in the study area. The inclusion of PC3 and PC4 increases the cumulative variance explained to 61.70%, demonstrating the additional influence of localized structural, mineralogical, and sedimentary processes. Comparable hierarchical controls, where lithology dominates the first component and weathering or structural processes influence subsequent components, have been widely reported in

airborne radiometric studies of basement and mixed terrains (Hasterok and Webb, 2017; Ahmed *et al*., 2019;) Artemieva *et al*., 2022; Karg *et al*., 2024). The PCA results therefore align well with established interpretations of radiometric datasets and confirm that radiogenic heat production in the study area is controlled by a combination of primary lithological composition and secondary geological processes.

Table 5: Principal component analysis of lithological unit for heat proximal sources

Lithological Units	Principal Components			
	PC1	PC2	PC3	PC4
A1	**0.553**	-0.515	-0.194	-0.087
A2	0.208	-0.176	**0.751**	-0.303
A3	**-0.519**	0.107	0.417	0.390
A4	0.454	-0.183	**0.585**	-0.100
W1	-0.365	**0.426**	0.119	0.145
W2	**0.567**	0.553	0.131	0.060
W3	**-0.681**	-0.307	0.134	-0.164
R1	0.107	-0.387	0.162	**0.792**
R2	-0.179	**0.664**	0.136	-0.111
R3	**0.733**	0.344	-0.042	0.221
Eigen value	2.323	1.632	1.213	1.002
% of Variance	23.226	16.319	12.133	10.02
Cumulative %	23.226	39.545	51.678	61.698

3.20 Hierarchical Cluster Analysis

The dendrogram, constructed using average linkage (between groups), provides a hierarchical clustering of the ten lithological units based on their radiogenic heat characteristics (Fig 17). Based on dendrogram patterns and PCA integration, three major clusters are identified: Cluster 1 (A1, A4) comprises highly radiogenic basement units that are distinct in composition and enriched in heat-producing elements. Cluster 2 (R3, A2, A3, W3) includes basement and weathered basement intermediate units, reflecting structural and mineralogical variability and localized enrichment or depletion effects. Cluster 3 (R1, R2, W1, W2) represents weathered and sedimentary units, primarily influenced by weathering, redistribution, and secondary concentration processes, exhibiting high similarity in radiogenic heat production. The clustering reveals patterns of similarity that align closely with the PCA findings, offering a complementary perspective on the controls of heat production.

At the smallest rescaled distances, R1 and R2 form the closest cluster, indicating highly similar radiogenic heat signatures. This observation is consistent with PCA, where both units show strong loadings on PC2, reflecting the influence of weathering and sedimentary redistribution processes. Similarly, W2 and W1 cluster closely, corresponding to their high PC1 loadings, which suggest enrichment in heat-producing elements (uranium, thorium, potassium). These patterns highlight that units influenced by weathering and sedimentary processes tend to form compact clusters due to their comparable radiogenic signatures. Intermediate clusters are observed with W3 and A3 joining at slightly higher rescaled distances, followed by the inclusion of A2 and R3, forming a larger group. PCA indicates that this group is influenced by both PC1 and PC3, capturing variability controlled by lithological composition and localized basement heterogeneity. Notably, A2 and R3, which show significant contributions to PC3, represent intra-basement variability, suggesting that structural or mineralogical factors drive their clustering. This cluster effectively illustrates the role of subtle lithological differences and localized enrichment/depletion effects within the basement units.

At the highest rescaled distances, A1 and A4 appear as outliers, joining the dendrogram only at high linkage distances. This observation aligns with PCA findings, where these units exhibit strong positive loadings on PC1, indicating radiogenically enriched, distinct lithologies. Their separation underscores the unique mineralogical composition of these units and their dominant influence on radiogenic heat production compared to other units.

The hierarchical clustering reinforces the PCA interpretation that radiogenic heat variability is controlled by multiple interacting factors rather than a single dominant influence. Basement units show clustering influenced by PC1 and PC3, reflecting intrinsic lithological and structural heterogeneity, whereas weathered and sedimentary units cluster according to PC2, highlighting the role of surface processes. Highly radiogenic units remain distinct due to their dominant PC1 loadings, underscoring unique enrichment in heat-producing elements. Collectively, the dendrogram and PCA analyses provide a consistent, complementary framework for understanding the controls of radiogenic heat production across diverse lithological units.

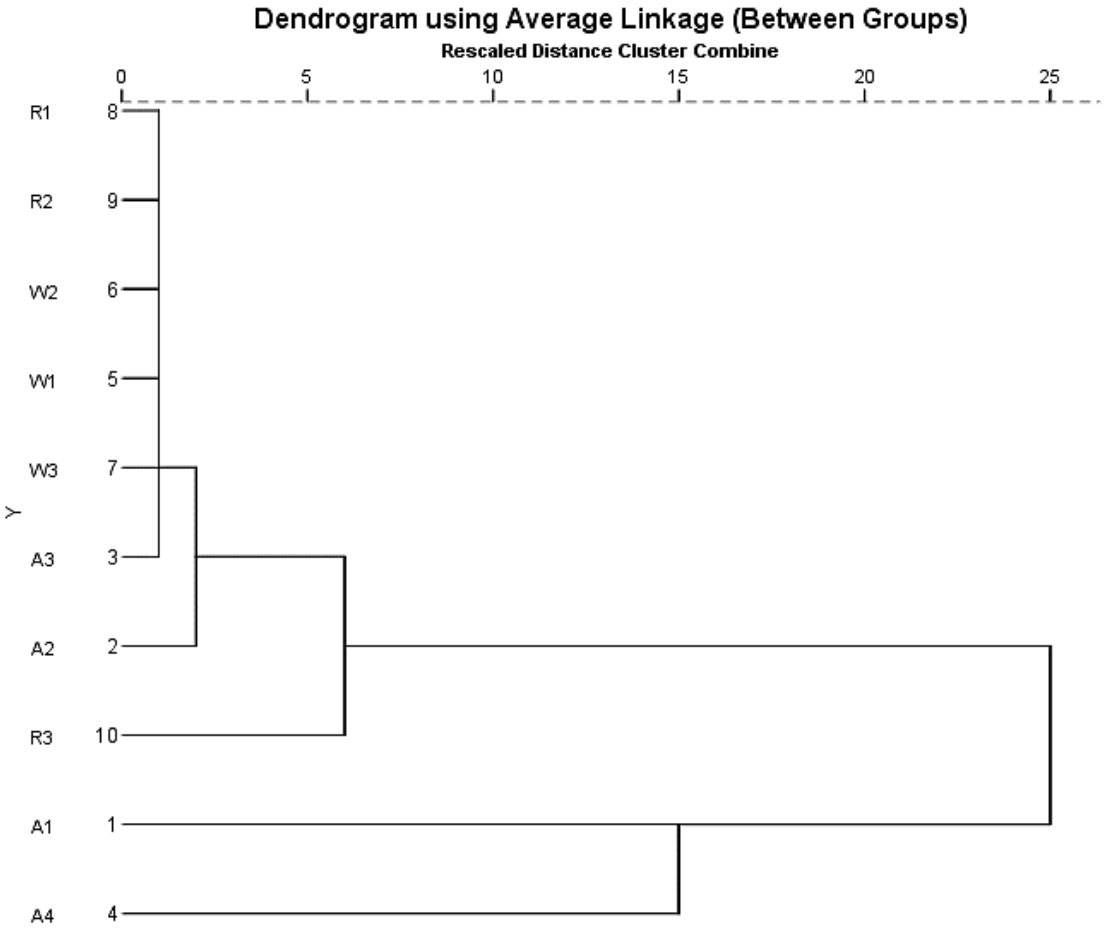

Fig. 17: Dendrogram representation of heat produced linkage across the lithological units

4.0 Conclusion

This study demonstrates that radiogenic heat production (HP) in Ogun State is predominantly controlled by lithology and mineralogical composition. Granitic and migmatitic basement rocks serve as primary heat sources, weathered basement units act as secondary concentrators, and sedimentary units reflect varying degrees of dilution or inheritance from underlying basement rocks.

Spatial analyses using 2D and 3D models reveal distinct high- and low-heat zones that correlate closely with mapped lithologies and structural trends, indicating the significant role of underlying basement structures in localizing heat anomalies. Most lithological units exhibit HP values above the IAEA recommended threshold of 4.0 $\mu W\ m^{-3}$, confirming the area's substantial geothermal potential, while only a few units fall below this limit.

Linear regression analysis further indicates that climatic factors such as temperature and relative humidity have negligible influence on HP, reinforcing the dominance of geological controls. The strong agreement between spatial lithological classification and statistical HP distributions underscores the robustness of the unit delineation

and confirms that radiogenic heat production across the study area is fundamentally controlled by lithology, degree of alteration, and sediment source history.

Based on these findings, targeted geothermal exploration should prioritize granitic and migmatitic basement terrains and their weathered equivalents, where heat production is highest. Sedimentary units with moderate HP should also be investigated for basement inheritance or localized geothermal exploitation. Detailed structural and geophysical mapping of faults, fractures, and lithological contacts is recommended to identify zones of concentrated heat more precisely. Integrating radiometric, geochemical, and geophysical datasets will enhance predictive modeling of heat production, supporting the sustainable development and utilization of geothermal resources in the study area.

Acknowledgements

The authors wish to emphatically acknowledge that this study is an Institutional Based Research (IBR), TETF/ES/DR&D/CE/UNIV/IJEBU-ODE/IBR/VOL.V 2024 sponsored by the grant received from the Nigeria Tertiary Institution Education Trust Fund (TETFUND), Abuja, Nigeria.

Conflict of Interest

The authors declare no known competing interest

References

Abbady, A. G. E., & Al-Ghamdi, A. H. (2018). Heat production rate from radioactive elements of granite rocks in north and southeastern Arabian Shield, Kingdom of Saudi Arabia. *Journal of Radiation Research and Applied Sciences, 11*(3), 281–290.

Ahmed, H. A., Shehta, A., Kamal, A., & Ren, M. (2019). Nature and evolution of the Precambrian lithosphere beneath the Arabian Shield of Saudi Arabia deduced from a suite of xenoliths from the Harrat Hutaymah Cenozoic volcanic field. *Lithos, 344–345*, 1–21.

Airo, M. L. (2002). Aerogeophysical interpretation of bedrock and regolith geology: Implications for gold exploration. *Geological Survey of Finland, Special Paper, 33*, 21–34.

Artemieva, I. M., Yang, H., & Thybo, H. (2022). Incipient ocean spreading beneath the Arabian Shield. *Earth-Science Reviews, 225*, 103918.

Artemieva, I.M., & Mooney, W. (2001). Thermal thickness and evolution of Precambrian lithosphere: A global study. *Journal of Geophysical Research: Solid Earth, 106*(B8), 16387–16414.

Artemieva, I.M., Thybo H., Jakobsen, K., Sørensen, N.K. & and Nielsen L.S (2017). Heat production in granitic rocks: Global analysis based on a new data compilation GRANITE2017. *Earth-Sci Rev*., 172, 1–26.

Ashwal., L.D, Morgan., P, Kelley., S.A. & and Percival J.A (1987). Heat production in an Archean crustal profile and implications for heat f low and mobilization of heat-producing elements. *Earth Planet Sci Lett.*, 85(4):439–50.

Bezuidenhout, J. (2023) Estimating geothermal and background radiation hotspots from primordial radionuclide concentrations in geology of South Africa. *J. Environ. Radioact.* 259–260: 107118.

Burton-Johnson, A., Dziadek, R., & Martin, C. (2020). Review article: Geothermal heat flow in Antarctica: Current and future directions. *The Cryosphere, 14*(11), 3843–3873.

Cooray, P.G., (1972). A Note on the Charnockites of the Ado- Ekiti Area, Western State, Nigeria". Geology of Africa T.F.J, Dessauvagie and A.J. Whiteman (eds.). 45-54. University Ibadan: Ibadan, Nigeria.

Dada, S.S., Lancelot, J.R., & Briqueu, L., (1989). Age and origin of the annular charnockitic complex at Toro, Northern Nigeria: U–Pb and Rb–Sr evidence. Journal of African Earth Sciences. 9, 227–234

Elueze A.A (1981). Petrography and geochemistry of metasedimentary rocks of the schist belt of Ilesha area, Southwestern Nigeria. Journal of Nigeria Mining and Geosciences Society, 18, 5-7.

Furlong, K. P., & Chapman, D. S. (2013). Heat flow, heat generation, and the thermal state of the lithosphere. *Annual Review of Earth and Planetary Sciences, 41*, 385–410.

Goodge, J. W. (2018). Crustal heat production and estimate of terrestrial heat flow in central East Antarctica, with implications for thermal input to the East Antarctic ice sheet. *Cryosphere* **12**: 491–504.

Haeger, C., Petrunin, A. G., & Kaban, M. K. (2022). Geothermal heat flow and thermal structure of the Antarctic lithosphere. *Geochemistry, Geophysics, Geosystems*, *23*(10), e2022GC010501.

Hasterok D, Gard M, & Webb J. (2018). On the radiogenic heat production of metamorphic, igneous, and sedimentary rocks. *Geosci Front*., 9(6), 1777–1794.

Hasterok, D., & Webb, J. (2017). On the radiogenic heat production of igneous rocks. *Geoscience Frontiers, 8*(5), 919–940.

Hazzard, J. A. N., & and Richards, F. D. (2024). Antarctic geothermal heat flow, crustal conductivity and heat production inferred from seismological data. Geophysical Research Letters, 51, e2023GL106274.

Hu J, Ma Y, Li Z, Wu Y, Gao, W, Peng, B, Wei, X. & and Liu D (2019). Jurassic sediments geochemical constraints on provenance, weathering process, and palaeoclimate variation of the north margin of Qaidam Basin, north-eastern Tibetan Plateau. *Geological Journal. 4*, 1–11.

International Atomic Energy Agency IAEA (2003) Guidelines for radioelement mapping using gamma-ray spectrometry data. IAE ATECDOC-1363, Vienna, Austria.

Jabbarova, L., Mustafayev, I., & Gasanalieva, N. (2024**)**. Effect of Temperature and Absorbed Dose on the Rate of Formation and Composition of Gaseous Products of Radiolysis of Bitumen-Bearing Rock. *Radiochemistry*, 65(6). 699-707.

Jaupart, C., Mareschal, J.C. & Iarotsky, L. (2016). Radiogenic heat production in the continental crust. Lithos 262, 398-427.

Karg, H., Paton, D., Salem, A., Alahmed, A., & Alraddadi, A. (2024). Effect of Precambrian basement structure on heat flow distribution in eastern Arabia. *International Journal of Earth Sciences*.

Markwick, P. J., Paton, D. A., & Mortimer, E. J. (2021). Reclus: A new database for investigating the tectonics of the Earth: An example from the East African margin and hinterland. *Geochemistry, Geophysics, Geosystems, 22*(11).

Minty, B. R. S. (1997). Fundamentals of airborne gamma-ray spectrometry. *AGSO Journal of Australian Geology and Geophysics, 17*(2), 39–50.

Ogunsanwo F.O, Adepitan J.O, Megba I. J, Osiyemi O.A. & Fowodu T.O. (2025). Heat production and seismic velocity in the basement lithology of Ago-iwoye, Ogun state, Nigeria. Dutse Journal of pure and applied Science 11(3), 133-151.

Ogunsanwo, F. O., Adepitan, J. O., Ayanda, J. D., Giwa, K. W., Falayi, E. O., & Adejimi A. I. (2021) Radiogenic heat production in crustal quarry rocks of Ogun State, south-western, Nigeria. Environmental Earth Sciences, 80:282.

Ogunsanwo, F.O, Ayanda, J.D, Mustapha, A.O, Olatunji, A.T, Ozebo, V.C, Olurin, O.T, Alaka, A.O, Okeyode, I.C, Adepitan, J.O, & Olowofela, J.A.(2023). Empirical Relation Between Magnetic and Radiometric Survey in Bitumen Area, Ogun State, Nigeria. *Materials and Geoenvironment*, 69 (2), 1 – 14.

Olowofela, J. A., Okeyode, I. C., Idowu, O. A., Olurin, O. T., & Ogunsanwo, F. O. (2019). Lithological mapping of Ogun State, Southwestern Nigeria, using aeroradiospectrometry. *Environmental Earth Sciences, 78*(7): 263.

Rahaman MA (1989). Review of the basement geology of South Western Nigerian. In C.A. Kogbe 2nd Ed. of Geology of Nigeria, Rock View, Jos, Nigeria. 39-56 pp.

Rahaman, M.A., (1976). Review of the basement geology of southwestern Nigeria. In: kogbe, C.A. (eds) geology of Nigeria, 2nd Ed. Elizabethan publication. Lagos, 41-58.

Rolandone, F., Lucazeau, F., Leroy, S., Mareschal, J. C., Jorand, R., Goutorbe, B., & Bouquerel, H. (2013). New heat flow measurements in Oman and the thermal state of the Arabian Shield and platform. *Tectonophysics*, *589*, 77–89.

Rudnick, R. L., McDonough, W. F., & O'Connell, R. J. (1998). Thermal structure, thickness and composition of continental lithosphere. *Chemical Geology*, *145*(3–4), 395–411.

Rybach, L., (1988). Determination of heat production rate. In: Hänel, R., Rybach, L., Stegena, I. (Eds.), Terrestrial Handbook of Heat-flow Density Determination. Kluwer Academic Publishers, Dordrecht, pp. 125-142. Ch. 4.2.

Salem, A., & Ali, M. Y. (2015). Mapping basement structures in the northwestern offshore of Abu Dhabi from high-resolution aeromagnetic data. *Geophysical Prospecting*.

Telford W.M, Geldart L.P, Sherif R.E, & Keys D.A (1990) Applied geophysics.Cambridge University Press, Cambridge

Vargas, C. A., Caracciolo, L., & Ball, P. J. (2022). Geothermal energy as a means to decarbonize the energy mix of megacities. *Communications Earth & Environment*, *3*(1), 66.

Vila, M., Fernández, M., & Jiménez-Munt, I. (2010). Radiogenic heat production variability of some common lithological groups and its significance to lithospheric thermal modeling. *Tectonophysics*, *490*(1–2), 152–164.

Wilford, J. R., Bierwirth, P. N., & Craig, M. A. (1997). Application of airborne gamma-ray spectrometry in regolith mapping. *Australian Journal of Earth Sciences*, *44*(2), 201–216.

Yusuf, A, Lim H.S, & Abir I. A (2023). Radiogenic heat production estimation towards sustainable energy drive in northeastern Nigeria. *Heliyo*n , 9 (6): e16310.